Spectroscopic Study of Strong Coupling between R6G-dye and optical cavities

Master's thesis, 23.6.2018

Writer:

Mikael Kautto

Instructors:

Jussi Toppari
Gerrit Groenhoff

UNIVERSITY OF JYVÄSKYLÄ

Abstract

Kautto, Mikael
Spectroscopic Study of Strong Coupling between R6G-dye and optical cavities
Master's thesis
Department of Physics, University of Jyväskylä, 2018, 62 pages.

When the energy levels of matter and optical environment are on resonance and the coupling between them is strong enough, the excited states of matter become inextricably linked with the modes of the local optical environment. The new energy levels of this strongly coupled hybrid light-matter system are very different from those of the matter or the optical system individually. The energy difference of these new states is called Rabi splitting. In spectroscopy the signature of strong coupling is the detection of Rabi split in absorption spectrum. This study demonstrates why Rabi split in absorption spectrum, originating from strong coupling between dye molecules and optical cavity, can not be explained by molecular absorption from cavity mode.

By evaporating silver layers, acting as mirrors, on above and below of a thin film it is possible to fabricate a low quality nanoscale optical cavity. With control of thin film's thickness, energy of the cavity mode can be made resonant with the electronic excitation of the dye molecules. Doping the thin film in between the mirrors with dye molecules creates a strongly coupled system, in which a Rabi split of hundreds of meV can be detected at room temperatures. Similar split can also be detected in transmittance spectra by adding dye doped thin films on top of a bare cavity. These films absorb part of the light, which is transmitted through cavity, without having an effect on reflectance spectra.

Optical cavities are simulated using the transfer matrix method. The structure of cavities are tuned to match the energy of $\lambda/2$ resonance mode with the electronic excitation of Rhodamine 6G (R6G) dye. Thicknesses of different layers are measured with atomic force microscope. Strongly coupled and reabsorbing systems are characterized with transmittance and reflectance measurements allowing calculation of the systems' absorption spectra. Optical measurements are made on different angles to find the dispersion of the systems. Calculated absorption spectra show a Rabi split only in the strongly coupled system. By increasing the concentration of R6G in cavity from 140 mM to 275 mM vacuum Rabi splitting is increased from 150 meV to 220 meV. Result agrees with theory, which states that vacuum Rabi split is linearly proportional to the square root of the concentration of the molecules.

Keywords: Strong coupling, optical cavity, reabsorption, Rhodamine 6G

Tiivistelmä

Kautto, Mikael
Spektroskooppinen tutkimus vahvasta kytkennästä R6G-väriaineen ja optisten kaviteettien välillä
Pro gradu -tutkielma
Fysiikan laitos, Jyväskylän yliopisto, 2018, 62 sivua.

Materiaalin viritystilat linkittyvät erottamattomasti paikallisen optisen ympäristön energiatilojen kanssa, kun materiaalin ja sen optisen ympäristön energiatilat ovat resonansissa ja kytkeytyminen niiden välillä on tarpeeksi vahvaa. Tällaisen vahvasti kytkeytyneen valon ja materian hybridin uudet energiatilat ovat hyvin erilaiset, kuin pelkän valon tai materiaalin energiatilat erikseen. Uusien energiatilojen erotusta kutsutaan Rabi jakautumiseksi. Spektroskopiassa absorptiospektrin Rabi jakautuminen on tunnusomainen piirre vahvalle kytkennälle. Tässä tutkielmassa havainnollistetaan, miksei väriaine-molekyylien ja optisten kaviteettien välisen vahvan kytkennän aiheuttamaa Rabi jakautumista pystytä selittämään spektrin jakautumisella, joka muodostuu väriaineen absorboidessa kaviteettimoodista.

Optiset Fabry-Perot kaviteetit luotiin höyrystämällä peilinä toimivat hopeakerrokset valoresiiniohutkalvon alle ja päälle. Lasin päälle luodut kaviteetit ovat satojen nanonetrien paksuisia ja niillä on leveät resonanssit. Säätämällä ohutkalvon paksuutta kaviteettimoodin resonanssienergia saatiin vastaamaan väriaineen elektronista viritysenergiaa. Lisäämällä väriainetta peilen väliseen ohutkalvoon muodostetaan vahvasti kytkeytynyt järjestelmä, josta voidaan mitata huoneen lämpötilassa satojen millielektronivolttien Rabi jakautuminen. Samankaltainen spektrin jakautuminen voidaan luoda transmittanssispektriin asettamalla väriainetta sisältäviä ohutkalvoja tyhjän kaviteetin perään. Lisätyt ohutkalvot absorboivat vain kaviteetin läpäissyttä valoa muuttamatta heijastusspektriä.

Optisia kaviteetteja simuloitiin käyttäen siirtomatriisimenetelmää. Kaviteettien rakenne optimoitiin siten, että kaviteetin $\lambda/2$-resonanssimoodin energia vastaa Rhodamiini 6G (R6G) väriainemolekyylin elektronista viritystä. Kaviteetin eri kerrosten paksuudet mitattiin atomivoimamikroskoopilla. Vahvasti kytkeytyneet ja uudelleenabsorboivat kaviteettijärjestelmät karakterisoitiin mittaamalla transmittanssi- ja heijastusspektrit. Järjestelmien absorptio laskettiin mitatuista spektreistä yhtälöllä $A = 1 - T - R$. Kaviteettien dispersiot selvitettiin tekemällä optiset mittaukset eri kulmilla. Ainoastaan vahvasti kytketyn järjestelmän absorptiospektreissä huomataan spektrin jakautuminen . Kasvattamalla R6G:n konsentraatiota kaviteetissa 140 millimoolista 275 millimooliin vakuumi Rabi jakautuminen kasvoi kiinteän kulman

absorptiomittauksessa 150 millielektronivoltista 220 millielektronivolttiin. Tulokset vastaavat teoriaa, jonka mukaan vakuumi Rabi jakautuminen riippuu lineaarisesti molekyylien konsentraation neliöjuuresta.

Avainsanat: Vahva kytkentä, optiset kaviteetit, uudelleenabsorptio, Rhodamiini 6G

Contents

1 Introduction

Interaction between light and matter can be divided into two regions: weak and strong coupling. Emission of a photon to continuum of radiation modes, when electron transitions from an excited state of atom or molecule to ground state, is an example of weak coupling. In the weak coupling regime the radiative properties of the molecule or atom can be altered. The quantum yield of emission and radiation rate constant of an excited state can be enhanced by so called Purcell effect [1] or the emission of the excited state can be inhibited totally [2]. Another weak coupling example is Förster energy transfer [3] between a donor and an acceptor atom or molecule.

When atom, or any system, interacts with its surrounding by weak coupling, the energy levels or frequencies do not practically shift and the system can be treated with perturbation theory. When the interaction becomes strong enough the energy levels responsible for the emission are altered. System's excited states become inextricably linked with the modes of the local optical environment. The new energy levels of this hybrid light-matter system, which is called polariton, are very different from those of the emitter or the optical system individually. This situation is known as strong coupling [4].

Relative new interesting achievements with strong coupling are strong coupling of cavity photons to a mechanical resonator [5], polaritonic coupling of Fabry-Perot cavity and the carbonyl stretch at an infrared frequency [6], strong coupling involving ground-state molecular vibrations in liquid phase [7], room temperature polariton condensates of cavity polaritons in microcavities filled with enhanced green fluorescent protein [8] and single molecule strong coupling [9]. Strong coupling has been used to control photochemical reaction rates [10] and work function of organic materials [11]. Strong coupling is a requirement for the preparation of squeezed and entangled quantum mechanical states or using mechanical resonators in the context of quantum information processing as quantum transducers [5]. Single-emitter strong coupling is believed to form building blocks for quantum information systems and for ultralow-power switches and lasers [9].

For the first time strong coupling between light and matter was achieved in 1983 at microwave frequencies using Rydberg atoms in an optical cavity [12]. After successfully coupling single atom first in microwave and later in optical frequencies also Bose-Einstein condensates were formed [4]. In the beginning of 1990's quantum wells were introduced to microcavities. In 1992 the first observation of a polariton splitting in a Fabry-Perot cavity was made by Weisbuch *et al.* Rabi split was 2 meV

at up to 77 K in a semiconductor microcavity [13]. Lots of interest has also been been paid to the interaction between excitons and photons in microcavities [14, 15]. Strong-coupling effects were not expected to be observed for molecules, because of the large excitation linewidths which result from inhomogeneous broadening and the presence of vibronic states [16]. Yet, results were anticipated because large oscillator strengths are characteristic feature of molecules and thus huge Rabi splitting energies were expected.

First time strong coupling between semiconductor microcavity and organic molecules was achieved by Lidzey *et al.* in 1998 [17]. Observed vacuum Rabi splitting was 160 meV instead of tens of meV which had been achieved with semiconductor microcavities and quantum wells. Soon after that other dyes were coupled in microcavities [18] and cavity polariton emission was observed [16].

Polaritonic chemistry, which is defined as ability to modify chemical structure and reactions through the formation of polaritons [19], was first experimentally demonstrated by suppressing chemical reaction rates of spiropyran molecules in 2012 [10]. Ever since polaritonic chemistry has been a topic of interest for both experimental and theoretical research and thus far it has been shown to modify relaxation pathways [20], photochemical reaction rates [10], the work function of organic materials [11] and the energy of the ground state of the coupled system [21]. Strong coupling between organic materials and light results with unique optical and electronic properties [22]. Because hybridization is not limited to electronic transitions, vibrational transitions can be selectively perturbed at a given bond, granting new possibilities to change the chemical reactivity landscape and to use it as a tool in spectroscopy and (bio)molecular science [23].

Enhancement of the field is a prerequisite for observation of strong coupling and can be achieved using plasmonic particles [24, 25], surface plasmon polaritons supported on noble metal surface [26, 27], hole arrays [28, 11, 29] or microcavities [22, 30, 31, 10]. The purpose of cavities is to confine light to small volumes using resonant recirculation. Due to the confinement of light material can interact coherently with a cavity mode for a meaningful time [32]. Different kinds of optical cavities with varying confinement times have been discussed meticulously by Vahala [32].

A large variety of strong coupling phenomena between light and matter can be explained by coupled harmonic oscillators. The light field of a certain frequency is one of the coupled oscillators and a material (atom, molecule, semiconductor, protein etc) with a well-defined optical or vibrational transition is the other oscillator. Given the amount of time the theory of strong coupling has been understood and the experiments have been ongoing, it is surprising how often in literature measuring only transmittance or reflectance is assumed to be enough for confirmation of strong coupling [32] or Rabi splitting is measured from either one [33]. Already in 1990 it was shown by Zhu *et al* that the signature of strong coupling, a split in spectrum, can be explained purely classically for transmittance measurement [34]. As pointed out by Houdré: "A relevant physical parameter that can be used as ex-

perimental evidence of vacuum field Rabi splitting is absorption, neither reflectivity nor transmission are unambiguous parameters. This important point is, even now, often forgotten and led to repetitive erroneous claim by newcomers in the field." [35]

The aim of this thesis is to illustrate the spectroscopic differences between a strongly coupled dye molecules in cavity and a non-interacting cavity system, which has linear reabsorption causing a split in the spectrum. Cavities were chosen due to the ability to tune resonance energy with the thickness and refractive index of the medium. A big part of the actual work was optimizing the cavity structure to match the resonant condition and finding out how to maintain the certain thickness of the doped film with increasing dye concentration. The key idea of the optimization process will be presented in section 3. Prepared optical cavities have low quality factor of 14. Yet, they have sufficient light confinement to obtain strong coupling between light and matter at room temperatures. Similar strongly coupled systems have been achieved with cavities with quality factor ranging from 10-100 [36, 22, 21, 7, 30]. Ultra high quality cavities can have quality factor up to 10^9, for example in a whispering gallery [32].

Rhodamine 6G (R6G) was for its robustness and familiarity for the research group [37, 26, 38]. R6G is a highly fluorescing dye. R6G, like all rhodamine family dyes as well as widely used dyes fluorescein and Texas red, are xanthene derivatives [39]. Since R6G withstands its optical properties in high temperatures and even in electron beam lithography, the sample preparation in this study does not have an effect to the dye.

2 Theoretical background

This section first introduces reader to the transfer matrix method, an effective way to model the optical properties of multilayer thin film structures. Next optical Fabry-Pérot cavities and their properties are simulated using the transfer matrix method. Finally strong coupling in spectroscopy is discussed.

2.1 Reflection and Transmission of Multilayer Structures

The most used method in optics for analyzing multilayer structures is the transfer matrix method derived by Harbecke [40]. The transfer matrix method yields very good approximations for multilayer systems, which can be reduced to 1D problem, as is done in Fig. 1. With transfer matrices the optical properties, meaning reflectivity, transmission and absorption, of the multilayer structure can be calculated. Also modeling the electric field inside a cavity is possible [41].

In presented theory materials are assumed to be non-magnetic and isotropic. The layers are smooth, planar and uniform in x and y directions. Forward direction of waves is $+\hat{\mathbf{z}}$. The wavevector of light is in x-z plane if the incident light has an angle compared to the normal of the surface, or just on z axis on normal incidence. The electric field can be presented at any point as a superposition of forward- and backward moving waves as

$$\mathbf{E}(\mathbf{r}) = \mathbf{E}_f^0 e^{i\mathbf{k}_f \cdot r} + \mathbf{E}_b^0 e^{i\mathbf{k}_b \cdot r}, \tag{1}$$

in which $\mathbf{k}_f$ and $\mathbf{k}_b$ are the wavevectors for forward- and backward-moving waves, respectively, and $\mathbf{E}_f^0$ and $\mathbf{E}_b^0$ are constant vectors. In the presented geometry the wavevectors are related to the index of refraction n by

$$\mathbf{k}_f = \frac{2\pi n}{\lambda_{vac}} \left(\hat{\mathbf{z}} \cos\theta + \hat{\mathbf{x}} \sin\theta\right), \quad \mathbf{k}_b = \frac{2\pi n}{\lambda_{vac}} \left(-\hat{\mathbf{z}} \cos\theta + \hat{\mathbf{x}} \sin\theta\right), \tag{2}$$

where θ is the angle from the normal of the incidence plane and λ_{vac} is the vacuum wavelength.

Light with its electric field along the plane of incidence is called p-polarized and light with its electric field normal to the plane of incidence is denoted s-polarized

light. In our coordination for s-polarized light

$$\mathbf{E}_{f,s} = E_{f,s}\hat{\mathbf{y}}, \quad \mathbf{E}_{b,s} = E_{b,s}\hat{\mathbf{y}} \tag{3}$$

and for p-polarized light

$$\mathbf{E}_{f,p} = E_{f,p}(-\hat{\mathbf{z}}\sin\theta + \hat{\mathbf{x}}\cos\theta), \quad \mathbf{E}_{b,p} = E_{b,p}(-\hat{\mathbf{z}}\sin\theta - \hat{\mathbf{x}}\cos\theta). \tag{4}$$

For the normal incidence of light there is no difference between s- and p-polarized light since the electric field of both polarization travels parallel to the surface.

Considering a wave traveling from layer 1 to layer 2, there are three relevant wave amplitudes on each interface between the layers: the incident amplitude $E_{f,1}$, the reflected amplitude $E_{b,1}$ and the transmitted amplitude $E_{f,2}$. The reflection coefficient r is defined as the ratio between the reflected amplitude and the incident amplitude and the transmission coefficient t is defined as the ratio between the transmitted amplitude and the incident amplitude. The equations for r and t are given by Fresnel Equations

$$r_s = \frac{n_1\cos\theta_1 - n_2\cos\theta_2}{n_1\cos\theta_1 + n_2\cos\theta_2}, \quad t_s = \frac{2n_1\cos\theta_1}{n_1\cos\theta_1 + n_2\cos\theta_2} \tag{5}$$

$$r_p = \frac{n_2\cos\theta_1 - n_1\cos\theta_2}{n_2\cos\theta_1 + n_1\cos\theta_2}, \quad t_p = \frac{2n_1\cos\theta_1}{n_2\cos\theta_1 + n_1\cos\theta_2}. \tag{6}$$

In the structure shown in Fig. 1 we have N materials with thicknesses L_n and refractive indexes n_n. The first ($n = 0$) and last ($n = N - 1$) layers are assumed to be semi-infinite. At the interface between materials $(n-1)$ and n the amplitude of the wave on nth side heading forward is v_n and the amplitude of the wave heading backwards is w_n. Note that for the last layer $v_{N-1} = t$ and $w_{N-1} = 0$. Also v_0 and w_0 are not defined. From the definitions of r and t we arrive to

$$v_{n+1} = \left(v_n e^{ik_{z,n}L_n}\right) t_{n,n+1} + w_{n+1}\, r_{n+1,n} \tag{7}$$

$$w_n e^{-ik_{z,n}L_n} = w_{n+1}t_{n+1,n} + \left(v_n e^{ik_{z,n}L_n}\right)\, r_{n,n+1}, \tag{8}$$

in which $t_{n,n+1}$ and $r_{n,n+1}$ are the transmission and reflection coefficients for light heading from layer n to $n+1$. Using the Fresnel equations (5), for $n = 1, 2, ..., N-2$ it can be written

$$\begin{pmatrix} v_n \\ w_n \end{pmatrix} = M_n \begin{pmatrix} v_{n+1} \\ w_{n+1} \end{pmatrix}, \tag{9}$$

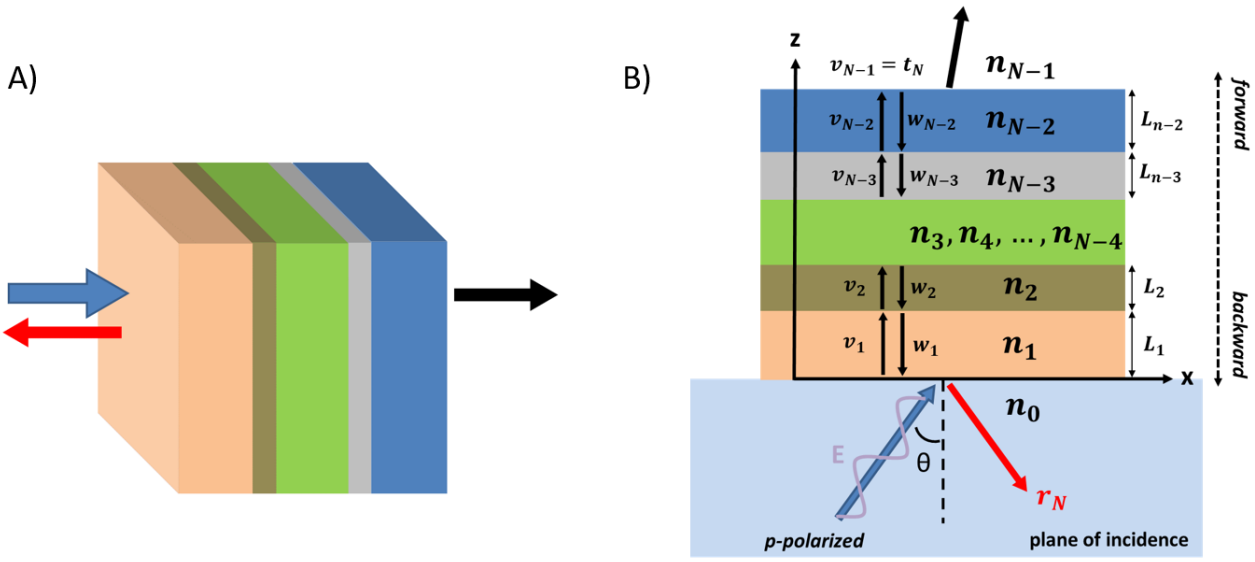

Figure 1. A) a multilayer structure which has stacked smooth, planar layers. Incident light (blue arrow) is reflected (red arrow) and transmitted (black arrow) through the structure B) reduced 1D structure of the multilayer system, which is treated in text.

where the transfer matrix M_n has the form

$$M_n = \begin{pmatrix} e^{-ik_{z,n}L_n} & 0 \\ 0 & e^{ik_{z,n}L_n} \end{pmatrix} \begin{pmatrix} 1 & r_{n,n+1} \\ r_{n,n+1} & 1 \end{pmatrix} \frac{1}{t_{n,n+1}}. \tag{10}$$

To describe the total field transformation from the incident waves to the waves transmitted through the multilayer system one has to take a product of N matrices of type M_n in the form

$$\begin{pmatrix} 1 \\ r_N \end{pmatrix} = \tilde{M} \begin{pmatrix} t_N \\ 0 \end{pmatrix}, \tag{11}$$

in which the system's transformation matrix $\tilde{M}$ is given by

$$\tilde{M} = \frac{1}{t_{0,1}} \begin{pmatrix} 1 & r_{0,1} \\ r_{0,1} & 1 \end{pmatrix} M_1 M_2 \cdots M_{N-1}. \tag{12}$$

Equation (11) can be written with four entries of the matrix $\tilde{M}$

$$\begin{pmatrix} 1 \\ r_N \end{pmatrix} = \begin{pmatrix} \tilde{M}_{00} & \tilde{M}_{01} \\ \tilde{M}_{10} & \tilde{M}_{11} \end{pmatrix} \begin{pmatrix} t_N \\ 0 \end{pmatrix}. \tag{13}$$

Therefore

$$r_N = \frac{\tilde{M}_{10}}{\tilde{M}_{00}}, \quad t_n = \frac{1}{\tilde{M}_{00}}. \tag{14}$$

The transmitted and reflected intensities, T and R, are found to be [42]

$$T_s = |t|^2 \frac{Re[n \cos\theta]}{Re[n_0 \cos\theta_0]} \tag{15}$$

$$T_p = |t|^2 \frac{Re[n \cos\theta^*]}{Re[n_0 \cos\theta_0^*]} \tag{16}$$

$$R = |r|^2, \tag{17}$$

$$\tag{18}$$

in which T_s is for s-polarization and T_p is for p-polarized light.

2.2 Optical Fabry-Pérot cavities

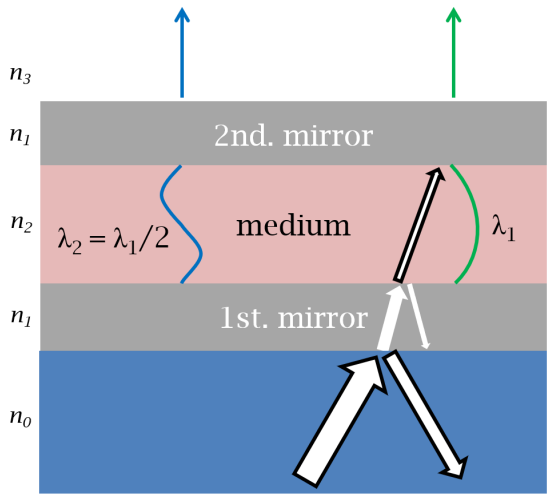

Figure 2. Plane parallel, or Fabry-Pérot cavity. White light is incident to the cavity from the bottom. At each interface part of the light is reflected and part is transmitted. Standing waves are formed inside the cavity and part of the resonance wavelength is transmitted through the structure.

Fabry-Pérot cavity, also called plane-parallel cavity, is an arrangement of medium in between parallel mirrors. Only electromagnetic waves with constructive interference form standing waves, resonance modes, inside the cavity. These modes are proportional to integer multiple m of $\lambda/2$ in the medium material. Especially in low quality cavities the thickness L and refractive index n at resonance wavelengths are not equal to $2Ln/m$ inside the medium material, since the electromagnetic waves penetrate inside and through the mirrors. Even in this case, the resonance modes of cavities are easily calculated using the transfer matrix method. A simple Fabry-Pérot cavity, which is simulated in this chapter, is seen in Fig. 2.

Example cavity consists of two silver mirrors with refractive index n_1 and a medium with refractive index n_2 between the mirrors. The values of refractive index for silver are obtained from [43]. The medium is photoresist and has refractive index 1.52. In all following graphs the bottom of system is semi-infinite layer of glass with dispersionless refractive index 1.52 and the top layer is air with refractive index 1.0. Layers are assumed to be homogeneous and scattering is not taken into account.

Using the transfer matrix method reflectance and transmission can be calculated at each interface and for the whole structure. An example transmittance spectra of optical cavity with silver layer thicknesses of 30 nm and medium layer thickness of 129 nm is seen in Fig. 3. The transmittance peak at 326 nm corresponds to silver's plasma frequency [10] and the peak at 550 nm origins from the resonance mode of the cavity.

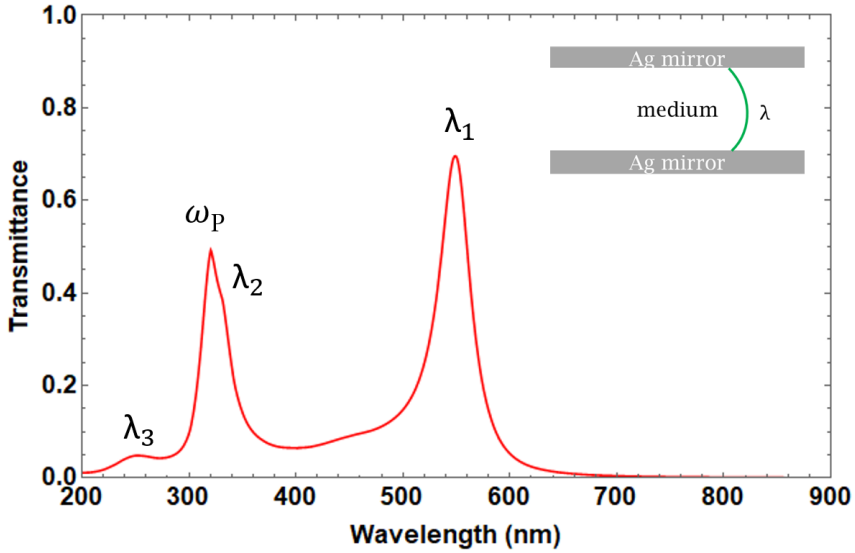

Figure 3. The transmittance spectrum of a cavity, which has 30 nm silver films as mirrors and 129 nm thin film as medium (refractive index 1.52). The peak at around 320 nm is due to silver plasma frequency ω_P. The transmittance peak λ_1 at 550 nm is due the first resonance mode, the shoulder close to plasma frequency at 330 nm is the second resonance mode λ_2 and the third resonance mode λ_3 is seen below plasma frequency at 250 nm.

The thickness of the layer in between the mirrors effects the resonance mode of the cavity. The thicker the cavity is, the longer forming standing wave is and thus resonance mode shifts to longer wavelengths. This effect is illustrated in Fig. 4, in which the medium between 30 nm silver films is changed from $L_1 = 130$ nm to $L_2 = 200$ nm. With 130 nm thick thin film cavity supports only the first resonance mode ($m = 1$, $\lambda_1 \propto 2L_1$), which has maximum wavelength at 550 nm. Cavity with 200 nm thick medium has the first resonance mode $\lambda_1 \propto 2L_2$ at 760 nm. The second resonance mode ($m = 2, \lambda_2 \propto L_2$) fits also within visible range and has maximum wavelength at 385 nm. The thicker medium in between mirrors is, the more standing wave modes can fit invisible range.

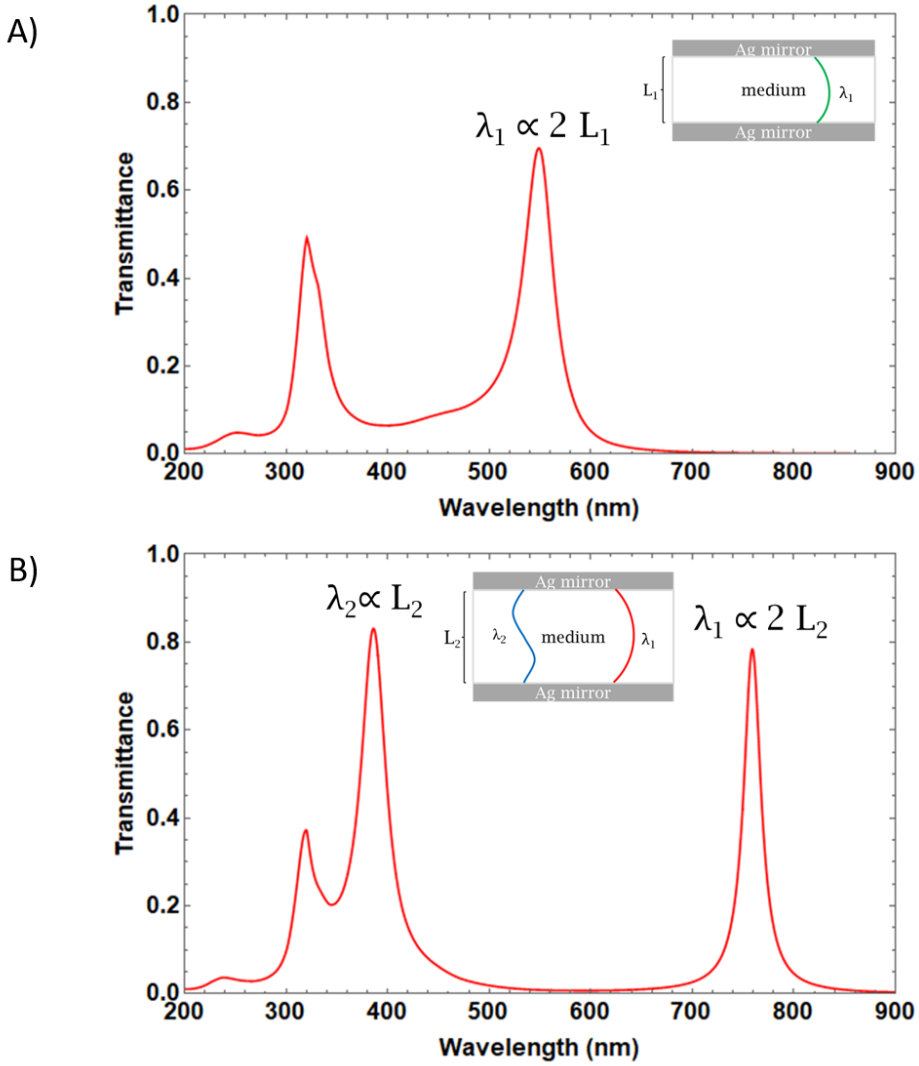

Figure 4. Cavity with medium thickness A) $L_1 = 130$ nm and B) $L_2 = 200$ nm. Silver layer thickness are 30 nm. A) The standing wave λ_1 has resonance wavelength of 550 nm. B) 1st standing wave λ_1 has resonance wavelength of 760 nm and the 2nd standing wave λ_2, has a resonance wavelength 390 nm.

The real part of the refractive index has exactly same kind of effect on resonance as thickness of the medium layer: the greater the value the higher wavelength the resonance mode has. The complex part of the refractive index, extinction coefficient, does not effect the resonance mode but makes medium absorb light. We shall return to absorptive material later in this chapter.

The thicknesses of the mirror layers have only slight effect on the resonance wavelength. Using the 200 nm thick medium and changing the thickness of silver layers from $t_1 = 30$ nm to $t_2 = 50$ nm the resonance wavelength of first mode decreases from 760 nm to 745 nm and the resonance wavelength of second mode decreases only from 390 nm to 385 nm, as is illustrated in Fig. 5. But increasing silver layer thickness has substantial effect on the quality factor of the cavity.

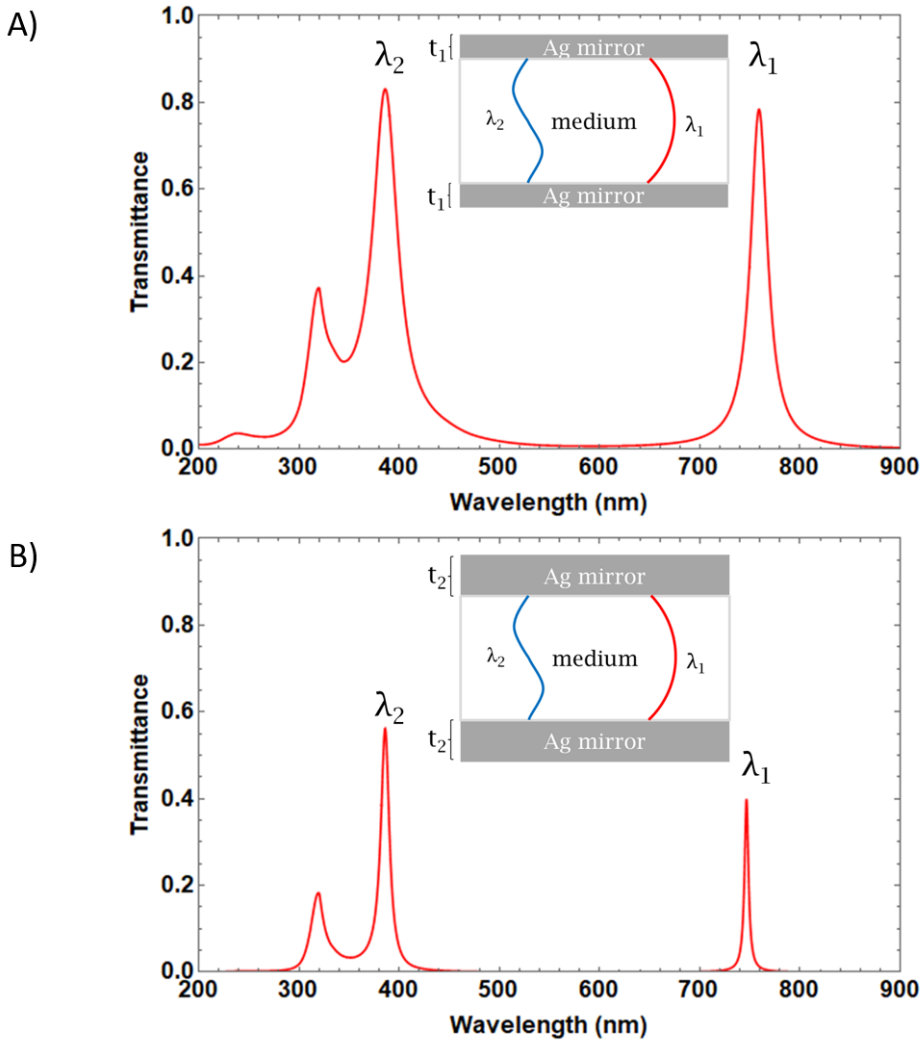

Figure 5. Cavity with silver 1 A) $t_1 = 30$ nm and B) $t_2 = 50$ nm. Medium thickness is 200 nm. The resonance wavelengths have only minor decrease but the transmittance decreases and peaks get narrower (FWHM decreases), which increases the quality factor of the cavity.

An ideal cavity would confine light indefinitely and would have resonant wavelengths at precise values. Deviation from the ideal condition is described by the quality factor (Q factor), which is defined as

$$Q = \frac{f_r}{\Delta f}, \tag{19}$$

in which f_r means the resonance frequency and Δf is the resonance width [44]. Resonance width is defined from a full width at half maximum (FWHM). Therefore by increasing the thickness of the silver mirrors the width of resonance peak and its FWMH decrease and the quality factor of the cavity increases. Another way of defining Q-factor is via energy storage:

$$Q = 2\pi \frac{E_{stored}}{E_{lost\,per\,cycle}}. \tag{20}$$

Both definitions become equivalent when Q-factor is high.

Knowing the basic properties of cavities we will consider reflectance and absorption of cavities. Like transmittance, reflectance can be calculated using the transfer matrix method. Absorption (A) of the sample can be calculated from transmittance (T) and reflectance (R) as

$$A = 1 - T - R. \tag{21}$$

Because light travels multiple times inside the medium there is high change, that at some point photon gets absorbed either by medium or mirror material even with low or non existing extinction coefficient. The transmittance, reflectance and absorption of a cavity with 38 nm silver films and 129 nm thick medium with refractive index of 1.52 are shown in Fig. 6. According to the simulation such cavity absorbs 40% of the incident light at the resonance mode.

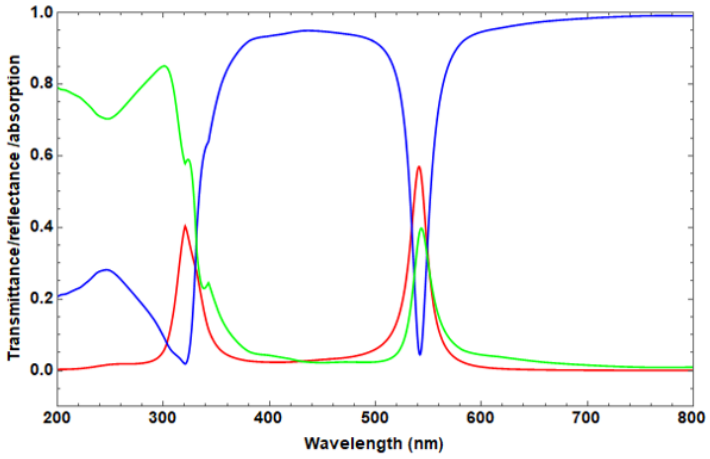

Figure 6. (Red curve) transmittance, (blue curve) reflectance and (green curve) absorption of cavity with 38 nm silver films and 129 nm thick medium with refractive index of 1.52.

So far we have only dealt with light incident at the normal of the cavity. Cavities have dispersion relation because the angle of incident light effects the resonance condition, as can be seen from Fresnel equations (5). Intuitive thinking would easily deduct that the increasing angle of incidence lowers the energy of the resonant wave, because the optical length is longer with an increased angle. This is not the case in reality! The waves interfere inside the cavity, meaning that all nonresonant waves disappear due to the destructive interference. The energy of the transmitted waves with an angle are increased due to the constructive interference. As pointed out by Skolnick *et al.*, the energy of cavity photon is approximately [41]

$$E = \frac{\hbar c}{n_c} k = \frac{\hbar c}{n_c} \sqrt{\left(\frac{2\pi}{L_c}\right)^2 + k_{||}^2} \,. \tag{22}$$

Dispersion of a cavity can be calculated with the transfer matrix method. A dispersion relation of a cavity with with medium thickness of 130 nm, refractive index of 1.52 and silver mirrors of thickness 38 nm can be seen in Fig. 7.

Also polarization of the incident light effects the reflectance and transmittance as is stated in Fresnel equations (5). Measuring the same cavity with *s*- and *p*-polarized light induces different dispersions, as can be seen from Fig. 8

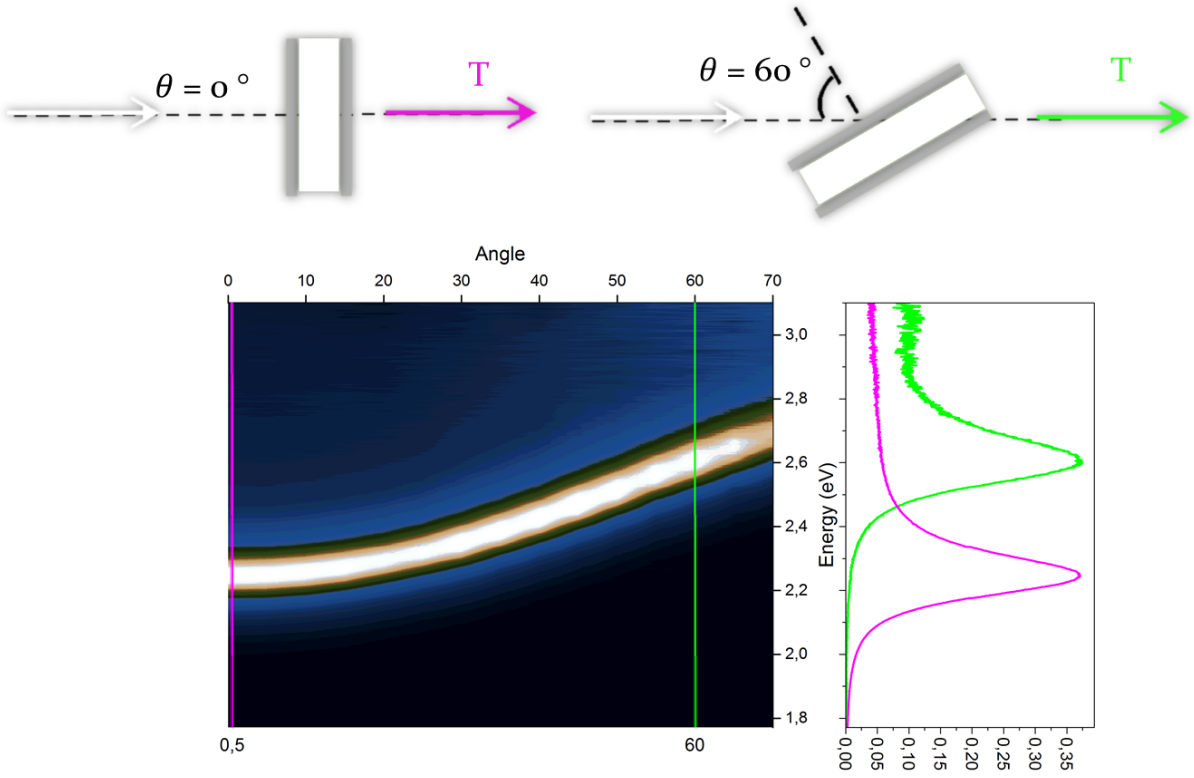

Figure 7. The dispersion of a cavity with medium thickness of 130 nm, refractive index of1.52 and silver mirrors with thickness 38 nm.

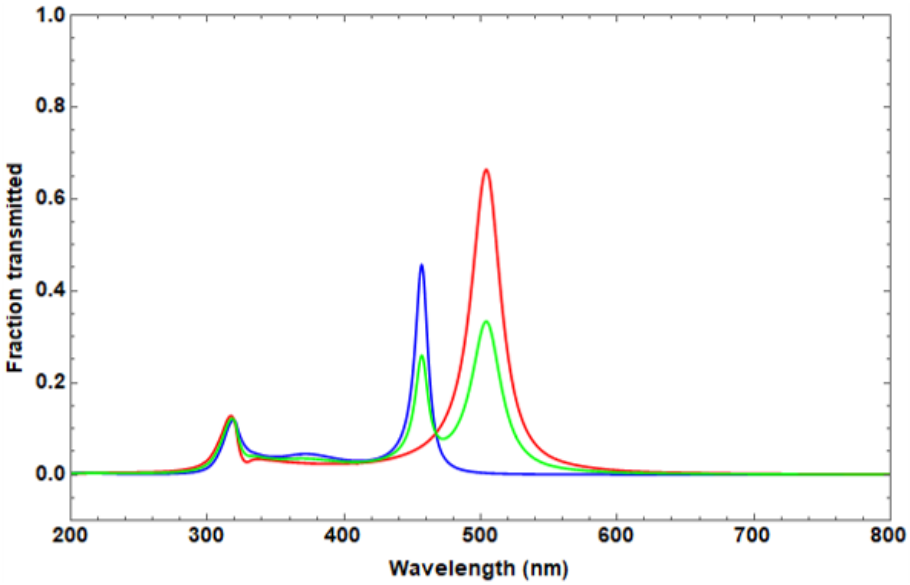

Figure 8. Transmittance spectra of cavity with 60° incident light having (blue curve) *s*-polarization, (red curve) *p*-polarization and (green curve) unpolarized light.

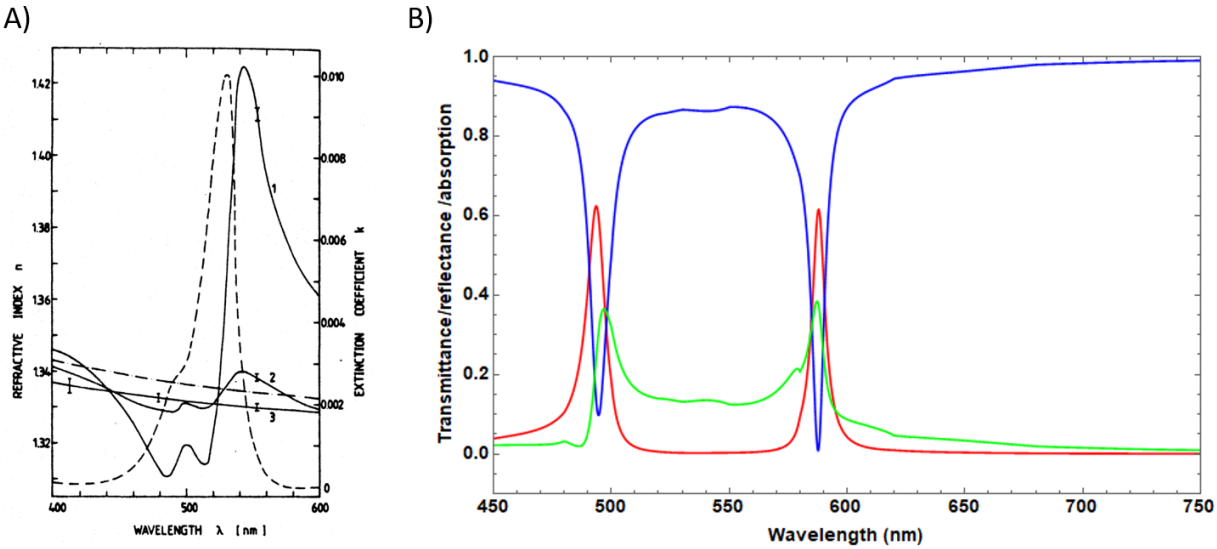

Figure 9. A) (Solid curves) (1) 0.1 M R6G in methanol (2) 0.01 M R6G in methanol, (3) pure methanol, (dash-dot curve) dispersion of water and (dashed curve) extinction coefficient of 0.01 M R6G in methanol. Figure reprinted from [45] B) Cavity, which has material with R6G refractive index with concentration 0.1 M as medium showing (red curve) transmittance, (blue curve) reflectance and (green curve) absorption.

When medium absorbs light the extinction coefficient is nonzero. Checking refractive index for 0.1 M R6G in methanol measured by Leupacher *et al.* [45] the real part of refractive index is in between 1.3 and 1.42. The imaginary part has maximum 0.01 with concentration 0.01 M R6G. Since absorbance is linear to the increase of concentration the extinction coefficient increases almost linearly when increasing concentration of R6G to 0.1 M. Simulation of cavity with 0.1 M R6G as a medium between 39 nm silver mirrors is seen in Fig. 9. Simulation shows a split in spectra, which can be due actual strong coupling in the system or purely linear reabsorption of the material, as is discussed in the next chapter.

2.3 Light-matter strong coupling in spectroscopy

Strong coupling can be achieved when the energy levels of coupled systems are close enough and there is sufficient coupling between the systems. The most familiar example of a strongly coupled system comes from chemistry, when the all electronic coupling between atoms' transition dipole moments gives rise to new eigenstates and leads to formation of molecules. The exactly same principle is applied to a situation in which molecules are placed inside an optical cavity, which is tuned to a given molecular electronic transition. In this quantum electrodynamics picture optical cavity is an oscillator with its own zero-point energy [2]. Schematic diagram of strong coupling between molecules and cavity is shown in Fig. 10. The hybrid states created in strong coupling of light and matter are called polaritons. The cavity quantum electrodynamics treatment predicts that the eigenstates of the system are no longer the molecule and cavity oscillator states but two mixed symmetric and antisymmetric states, which have wave functions [23]

$$|P+\rangle = c_{11}|e\rangle_m|0\rangle_c + c_{12}|g\rangle_m|1\rangle_c \tag{23}$$
$$|P-\rangle = c_{22}|e\rangle_m|0\rangle_c - c_{21}|g\rangle_m|1\rangle_c, \tag{24}$$

where molecule is in the excited state (e) with 0 photons in the cavity or the molecule is in the ground state (g) with 1 photon in the cavity. Polaritons are separated by Rabi splitting energy.

As explained by Haroche *et al.* [2], when there is no dissipation the Rabi splitting energy $\hbar\Omega_R$ between hybrid light and matter states is given by the product of the electric field amplitude E in the cavity and the transition dipole moment d

$$\hbar\Omega_R = 2Ed\sqrt{n_{ph}+1} = 2d\sqrt{\frac{\hbar\omega}{2\epsilon_0 V}}\sqrt{n_{ph}+1} \tag{25}$$

in which $\hbar\omega$ is the cavity resonance, ϵ_0 the vacuum permittivity, V the mode volume and n_{ph} the number of photons in the cavity. Equation (25) assumes transition dipole moment being a two-level system, which is at resonance with a cavity mode. As pointed out by Hutchison *et al.*, even when n_{ph} goes to zero, there remains a finite

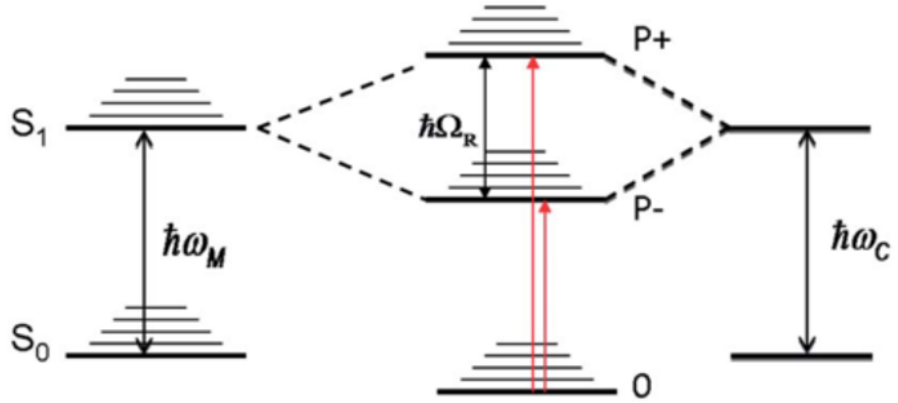

Figure 10. A schematic picture of strong coupling between molecular transition $\hbar\omega_M$ and a cavity mode $\hbar\omega_C$, which form hybrid light-matter eigenstates, polaritons, $P+$ abd $P-$. Rabi splitting between polaritons is shown as $\hbar\Omega_R$. Figure reprinted from [36].

value of vacuum Rabi splitting, $\hbar\Omega_{VRS}$, where the zero-point energies of the molecular and optical transitions generate the new light-matter states [10]. When molecule and 'vacuum field' couple the result is a quantum of energy shifting back and forth between the molecule and the cavity mode at the vacuum Rabi frequency [32]. Rabi splitting is itself proportional to the square root of the number of molecules in the cavity $\sqrt{n_{mol}}$ [2], which implies that vacuum Rabi splitting is proportional to the concentration of molecules as [10]

$$\hbar\Omega_{VRS} \propto \sqrt{\frac{n_{mol}}{V}}. \tag{26}$$

The volume V of an electromagnetic mode in a cavity is quite enormous ($\sim \lambda^3$ or μm^3 at visible) compared with the volume occupied by a molecule ($\sim nm^3$), making it possible for numerous molecules to interact with the mode, which results in a significant enhancement of the Rabi splitting [23]. On top of the amount of the molecules, the structure of cavity and the location of molecules inside the cavity effect the size of Rabi splitting. As discussed in previous section 2.2 only modes $m\lambda/2$, with integer number m, form standing waves in cavity. In Fig. 11, made by Wang *et al.*[22], a layer of dye doped film is located at different positions in $\lambda/2$-cavity and λ-cavity. The Rabi splitting of evenly dispersed molecules in $\lambda/2$ -cavity is greater than Rabi split in a slab of film containing dye molecules located at node of field amplitude in λ-cavity. The strongest Rabi split is obtained by placing a molecular layer at the antinode of smallest mode volume cavity. For simplicity of cavity preparation, molecules are evenly dispersed in the cavity in this thesis.

In order to observe strong coupling the molecule-cavity coupling must be larger than the molecule and cavity relaxation rates. The lifetime of photon in cavity is finite due to finite quality factor, which limits Rabi oscillations by allowing energy to leak

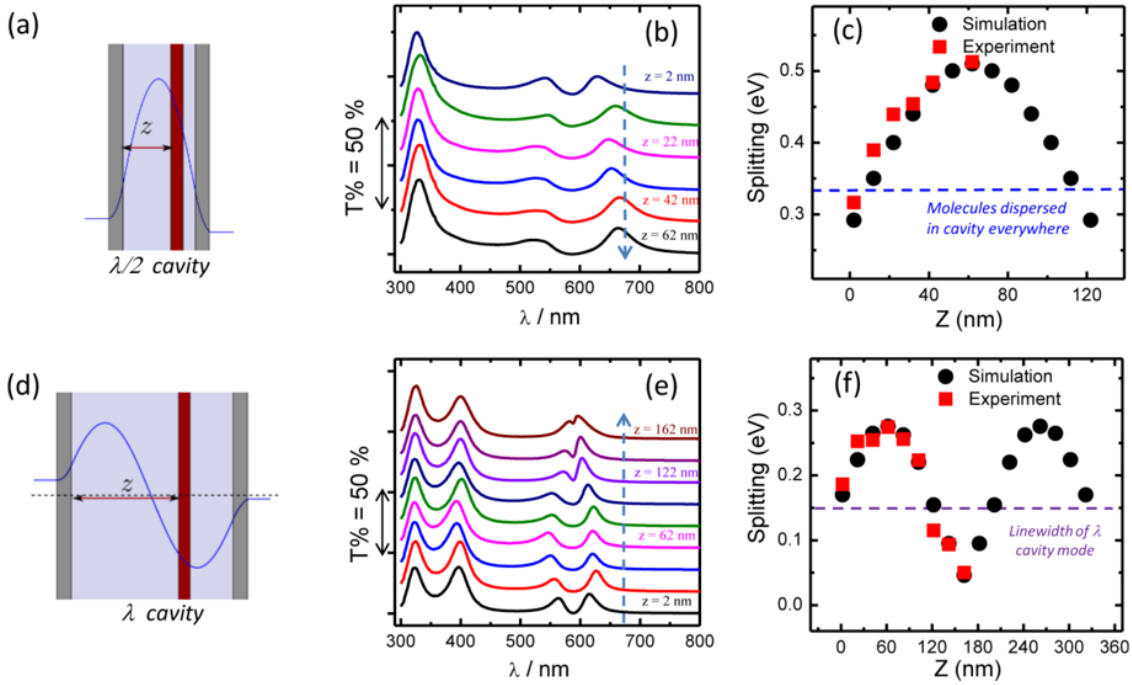

Figure 11. a) Schematic representation of the $\lambda/2$-cavity and the corresponding field amplitude. (b) Transmission spectra of a set of $\lambda/2$-cavities resonant with a TDBC molecular layer located at different spatial positions inside the cavity (c) Rabi splitting (red squares) versus spatial position of the molecular layers inside the $\lambda/2$-mode cavities. Blue dashed line represents the $\hbar\Omega_R$ when the molecules are dispersed evenly inside the cavity. (d) Schematic representation of the λ-cavity and the corresponding field amplitude. (e) Normal incidence transmission spectra of a set of λ mode cavities with TDBC molecular layer and (f) their corresponding $\hbar\Omega_R$ (red squares) at different spatial positions inside the cavity. The purple dashed line indicates the FWHM line-width of the $\lambda/2$-mode (150 meV) as the minimum energy splitting below which strong coupling can no longer be defined. Figure reprinted from [22].

irreversibly into the continuum. Also the molecule transition couples to continuum radiation modes and thereby experience spontaneous decay. Strong coupling can occur when the molecule–photon coupling strength is faster than any dissipative rate and larger than $1/T$ where T is the interaction time [46]. Therefore strongly coupled systems can be defined as systems, in which the Rabi dynamic can exist despite dissipation.

When the Rabi split becomes a fraction of the transition energy $\hbar\omega_m$, the perturbation of the coupled system is so strong that the energies of the other states of the system are modified [36]. This is the so-called ultra-strong coupling regime where the ground state energy of the system shifts, as has been observed experimentally [21]. I shall concentrate on strong coupling regime with the pragmatic definition of strong coupling from Törmä's article: "the system is in the strong coupling regime

whenever the Rabi split is experimentally observable" [4]. Ultra-strong coupling is discussed in more detail in literature [36, 47].

Measurement of the dispersion of strongly coupled system should always be done by measuring the wavelength or frequency with constant k-vector, which is a function of the angle of incident light. This scan is called λ- or ω-scan depending on the variable. The opposite and wrong method would be measuring the k-vector (meaning the angle of incident light) with a fixed energy. This scan is called k-scan and results in back bending and incorrect interpretation of the data, as was shown by Pockrand *et al.* [48]. Point is illustrated well in Fig. 12.

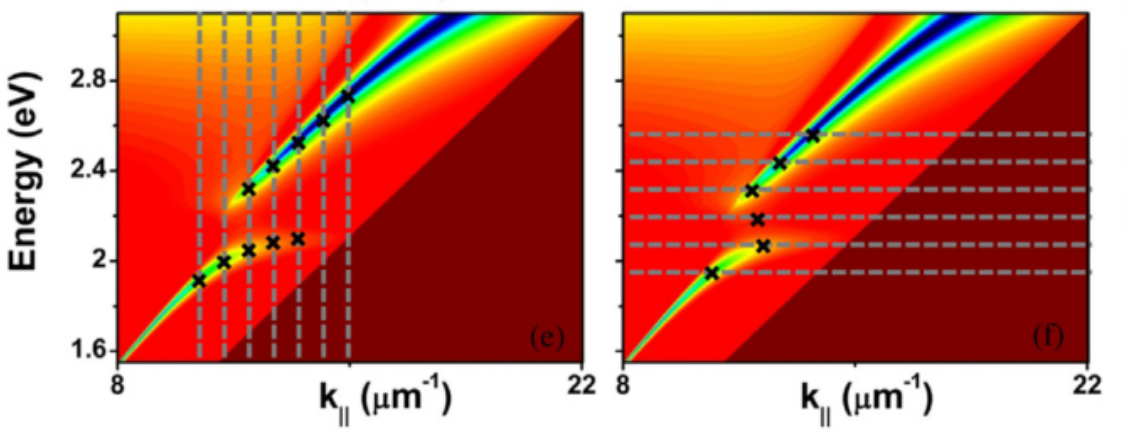

Figure 12. The vertical/horisontal lines depict wavelength /wavevector scans, respectively: the minima determined from these scans differ as is shown by the black crosses. Figure is reprinted from [4].

As pointed out by Savona [49] the necessary condition to observe an anticrossing behaviour is different for reflectivity, transmission and absorption spectrum. Yet, only detecting split in absorption spectrum proves actual existence of strongly coupled system. The observation of a split in transmission or reflectance alone does not allow distinguishing a real normal mode splitting from an absorptive dip created in a broad Fabry–Pérot mode [35], as is shown in Fig. 13. Therefore observing split only in an empty cavity's transmittance or reflectance spectra can not distinguish quantum mechanical effects from merely the combination of linear absorption and dispersion [34].

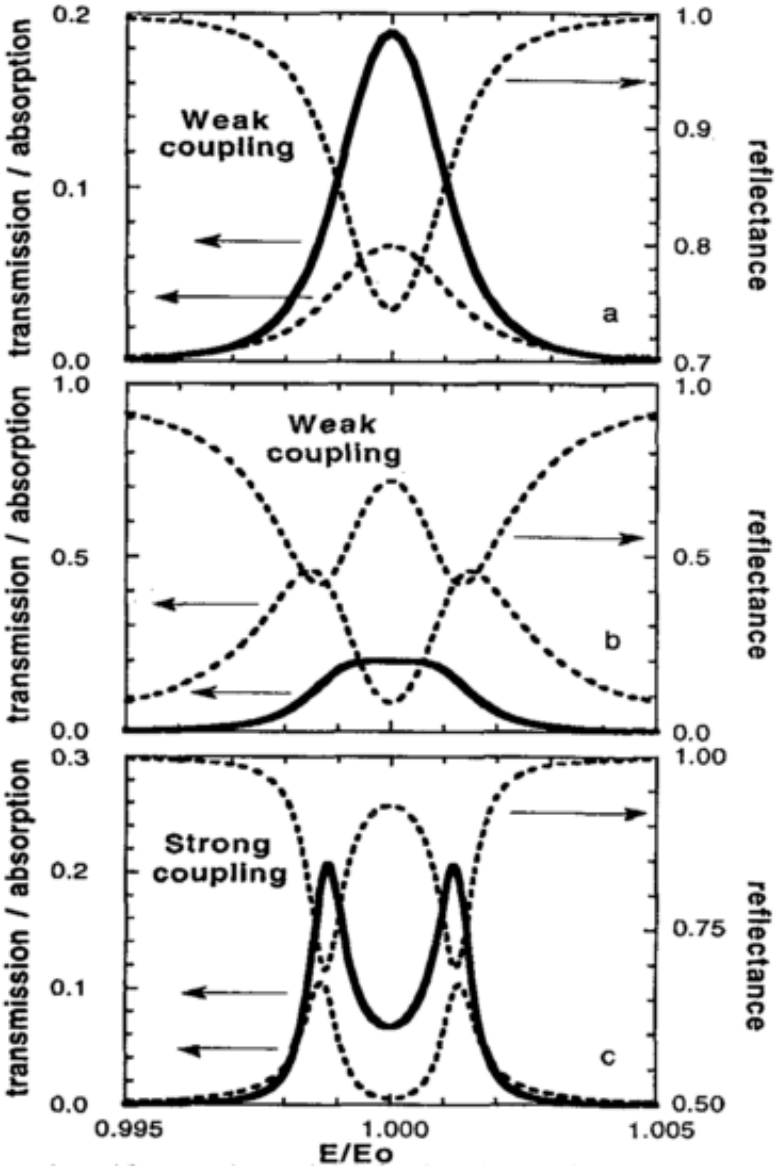

Figure 13. (Thick line) absorption, (dashed line) transmission and (dashed line) reflectance of a Lorentz oscillator in a cavity. On top image usual weak coupling regime. At center image a nonrelevant splitting is seen in transmission and reflectance but not in absorption. At bottom spectra a strongly coupled system, which has split in all spectra. Figure reprinted from [50].

3 Materials and methods

Materials and methods section first introduces the parameters used in the simulations of cavities. Next the preparation of thin films is presented following the preparation of cavities. Rest of the section is dedicated to optical measurement set-ups.

It is worthwhile reminding that while optimizing the cavity structure the parameters of both thin films and cavities were changed multiple times. Therefore the parameters of thin films were not fixed until functional cavities with good enough resonance were prepared. After fixing the properties of thin films the cavity structure was fine tuned to give most suitable optical properties.

3.1 Simulation parameters

Cavities were simulated with a n-layer code using the transfer matrix method with Mathematica. The optical constants for silver were obtained from work done by Johnson *et al.* [43]. The refractive index of R6G was obtained from Leupacher *et al.* [45]. The value of the refractive index for SU-8, 1.52, was obtained from a data-sheet [51]. Used refractive index for air is 1 and for glass is 1.52. Both glass and SU-8 are assumed to be dispersionless. Air and glass are treated as semi-infinite layers.

3.2 Thin film preparation

While preparing thin films the total amount of solid's in the solution was calculated and kept constant to have approximately same viscosity in all solutions. The solids in the solutions are the mass of R6G and the amount of solids in SU-8 solution. Same viscocity should yield same thickness of the thin film with same spinning parameters. The total solid content of solutions was fixed to 44.5 mg/ml. This amount of solids with the used spin parameters gave required thickness to thin films. Assuming that all solvent will evaporate during the bake, the ratio of R6G molecules to solids of SU-8 gives the concentration of the thin films. Therefore the mass of R6G was calculated from the needed ratio of R6G molecules to solids of SU-8 in the film. Knowing the required mass of R6G and solids in SU-8 the solution used in thin film preparation was diluted to total solid content of 44.5 mg/ml by adding cyclopentanone.

It should be noted that the concentrations of thin films are not exact, but give an idea of the order of magnitude of the concentrations we are dealing with.In all the cases the measured absorption of the thin film was used as the reliable measure of the R6G content. A detailed calculation of solution's solid contents and film concentrations are given in appendix A.

3.2.1 Preparation of solutions

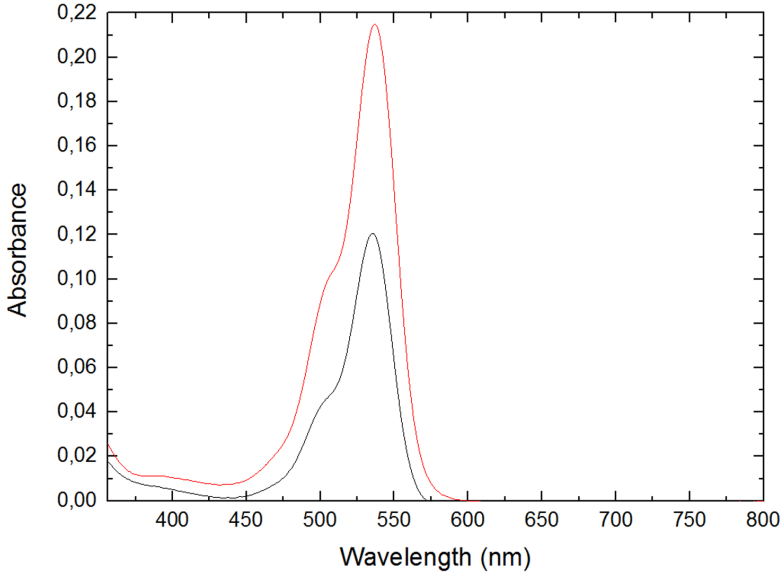

Figure 14. Absorbance of thin films with two different concentrations of R6G dye used in cavity preparation: (black curve) 140 mM R6G film and (red curve) 275 mM R6G film.

Rhodamine 6G can form aggregates with high concentrations especially in solvent form. The aggregates, called associates in the translated text of Levshin [52], have higher excitation energy than monomers and greater Stokes shift. Comparing absorbance of 140 mM and 275 mM R6G thin films, seen in Fig. 14, to the ones reported by Levshin, seen in Fig. 15, we can safely say that our molecules are still as monomers in thin films.

SU-8 root solution is prepared by weighing 1.984 g SU-8 2100 (SU-8 2100 MicroChem, Lot# 05080635) and dissolving it with 9.623 ml cyclopentanone (Fluka analytical, $>$ 99 % GC, Lot# 1382632 54408141, CAT 120-92-3). The mixing and storing of root solution are done in a glass flask. R6G solution is made by dissolving 4 mg R6G (R6G, also known as Basic Red 1, from Sigma-Aldrich, dye content 99% M_w = 479.01 g/mol, CAS: 989-38-8, Lot# MKBR1004V) to 300 µl ethanol (ETAX A, from Altia, min 94% vol.-%) making 28 mM R6G solution. To avoid aggregates in thin film, the well mixed solution was filtered with 0.2 µm pore size filters (Sartorius Minisart filter).

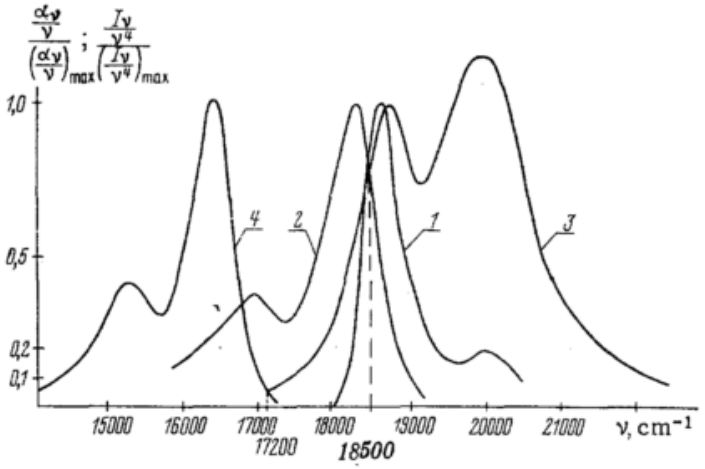

Figure 15. The frequencies of R6G absorption and emission in ethanol at temperature -175 °C. Absorption (1,3) and luminescence (2,4) spectra of monomers (1,2) and aggregates (3,4) with concentrations 10^{-5} and $5 \cdot 10^{-2}$ mole/liter, respectively. Picture reprinted from [52].

140 mM SU-8 thin films doped with R6G dye are prepared by mixing 75 µl 28 mM R6G in ethanol solution with 75 µl 28 mM R6G in ethanol to get 150 µl 14 mM R6G in ethanol solution. 170 µl cyclopentanone is added to easen the mixing of photoresist and dye solution. Finally 150 µl SU-8 root solution, which had been diluted 1:6 by volume with cyclopentanone, is added to base solution. Solution is mixed rigorously to dissolve SU-8 well.

For stronger concentration of 275 mM R6G doped thin film 150 µl 28 mM R6G in ethanol solution is mixed with 192 µl cyclopentanone. Finally 150 µl SU-8, which is first diluted 1:6 by volume with cyclopentanone, is mixed to the solution.

Solution for thin film without dye molecule is made by mixing 150 µl ethanol, 147 µl cyclopentanone and 150 µl SU-8 root solution (diluted 1:6 by volume with cyclopentanone). The solution is used in bare cavities and also to prepare the thin films protecting the top silver layer of cavities. The film recipes are summarized in table 1.

Table 1. The amounts of R6G solution, cyclopentanone and SU-8 root solution used in preparation of different thin film solutions.

	bare film	140 mM	275 mM R6G
ethanol (µl)	150	75	-
28 mM R6G in ethanol (µl)	-	75	150
cyclopentanone (µl)	147	170	192
SU-8 root solution (µl)	150	150	150

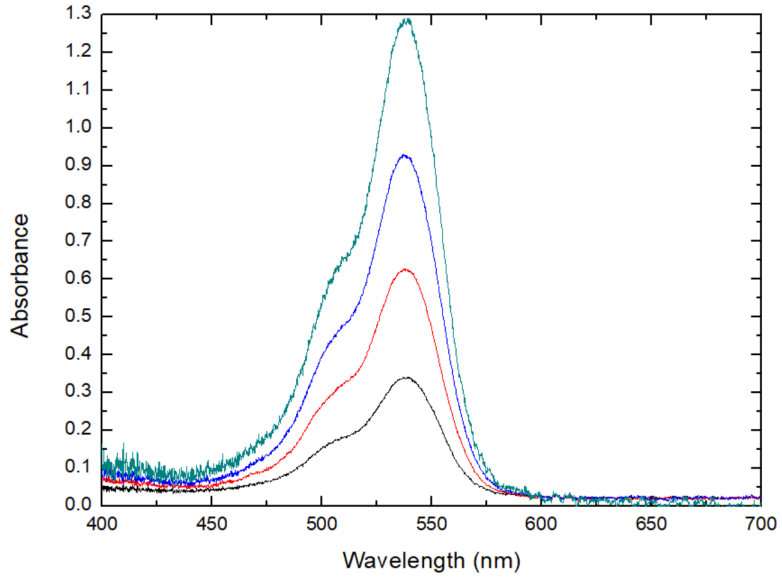

Figure 16. The absorbance of stacked R6G films used in reabsorption experiment. (Black curve) one thick 275 mM R6G film, (red curve) two similar films, (blue curve) three films and (cyan curve) four stacked 275 mM R6G films. The absorbance of glass substrates is subtracted from spectra.

3.2.2 Film characterization

To measure the absorbance and film thickness, the thin films are prepared on top of glass substrate, which is precision cut and unbevelled Floatglass made by Präzision Glas & Optik Gmbh. Thickness of glass is 1.25 mm and refractive index is 1.52 at 588 nm. The glass is cut to approximately 2 cm x 2 cm pieces, which are cleaned by rubbing them with cotton stick in heated acetone followed by sonication in isopropanol alcohol for 10 minutes. Glass pieces are dried by blowing with dry nitrogen flow.

Thin films are prepared on top of the glass with spinning rate of 6000 rpm and spin time of 60 seconds. After spin coating sample is soft baked on hot plate at ∼95° C for 3 minutes. Thin film is cured by illuminating sample with UV-lamp for 1 min. R6G film thicknesses are characterized by scratching the film with a scalpel and measuring the valley by KLA Tencor P-15 Profilometer. The thickness of prepared thin films on top of glass was tuned to 120 nm.

Absorbance of the prepared thin films were measured with UV-vis spectrophotometer (Perkin Elmer Lambda 650 UV/vis spectrophotometer). 140 mM film has maximum absorbance of 0.12 at 536 nm (2.31 eV) and 275 mM R6G film has maximum absorbance of 0.21 at 538 nm (2.30 eV), as can be seen in Fig. 14. These values are close to literature values of R6G absorption in ethanol solution having maxima at 530 nm (2.34 eV) [52, 45].

Thin films of reabsorption studies were prepared from the same solution as 275 mM R6G doped thin films, but the spin coating was made using spin speed 2000 rpm for 60 s to make a thicker film. Samples are soft baked on hot plate at ∼95° C for 3 minutes. Four such films were prepared for the sole purpose of absorbing the light passing through the empty cavity. Therefore thickness of these films isn't of interest and only absorbance was measured. Absorbance of the thick 275 mM R6G thin films stacked from one up to four films are seen in Fig. 16. The absorbance of glass substrates were reduced from spectra by subtracting absorbance of stacked glass substrates. Maximum absorbance of a single film is 0.338 at 538 nm (2.305 eV), with two films stacked absorbance increases to 0.626, with three films 0.930 and with four films absorbance increases to 1.284. The increase of absorption is close to linear.

3.3 Cavity preparation

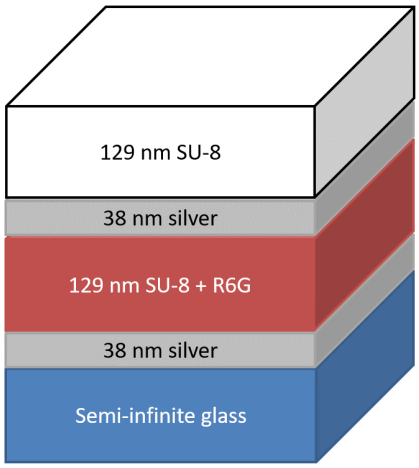

Figure 17. Structure of prepared cavities. Glass substrate is not to scale.

The structure of the prepared cavities is seen in Fig. 17. They are prepared on a glass substrate, which is prepared in a similar way as in section 3.2. Silver layer is evaporated on top of cut and cleaned glass in ultrahigh vacuum ($2 \cdot 10^{-8}$ mbar) using low evaporation rates of 0.02-0.04 nm/s to increase the smoothness of the layer. The thickness of silver layer was 38 nm. Thickness of evaporated film is characterized by scratching the film with a scalpel and measuring the depth of the valley with Veeco Dimension 3100 (Nanoscope IV) atomic force microscope (AFM). An example can be seen in Fig. 18.

Prepared SU-8 based solution, either with or without dye molecule, was spin coated at 6000 rpm for 60 seconds on top of the first silver layer as soon as possible after the evaporation. After spin coating sample is soft baked on hot plate at ∼95° C for 3 minutes. Thin film is cured by illuminating sample with UV-lamp for 1 min. The resist layer thickness is confirmed with AFM scratch measurement, which can

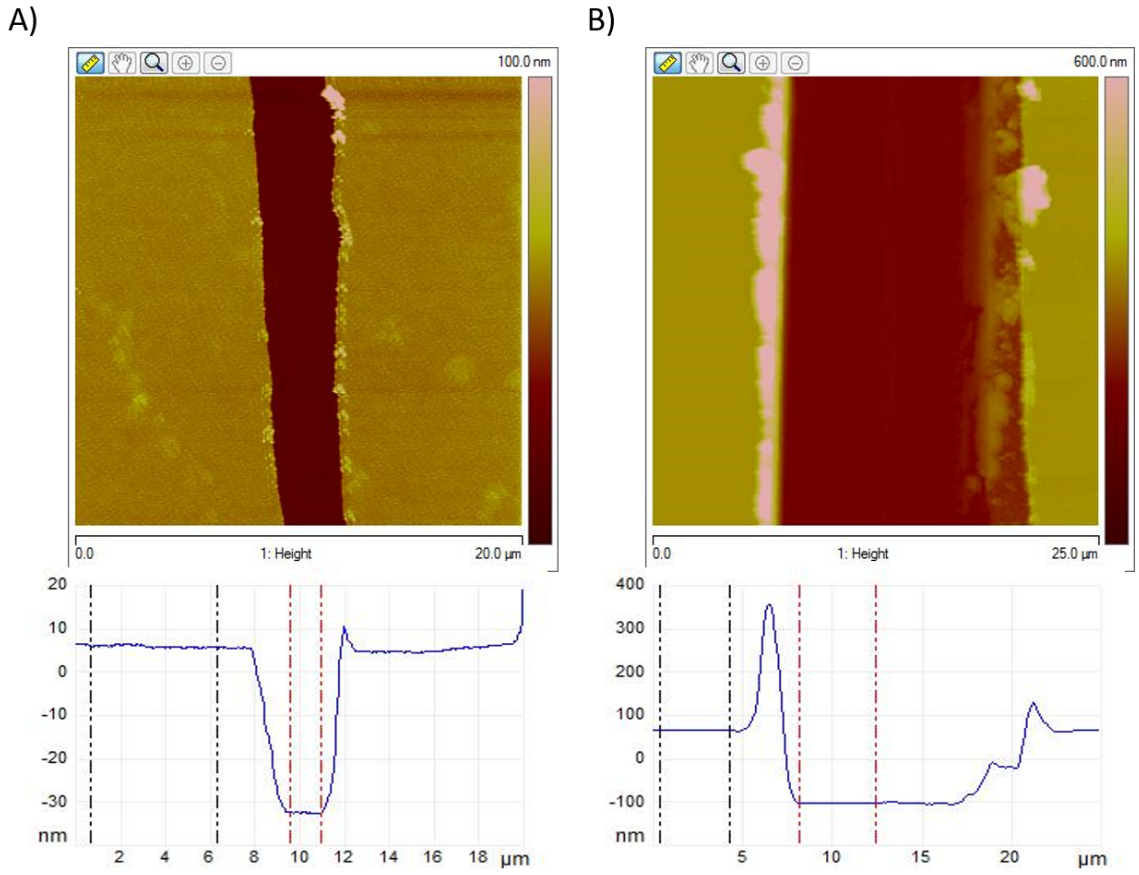

Figure 18. AFM image of A) an evaporated silver layer, which has thickness of 38 nm and B) the spin coated thin film and silver layer, which has total thickness of 167 nm. Therefore the thickness of the resist layer is 129 nm. Averaged cross sections are shown below the images.

be seen in Fig. 18. During AFM measurements I noted that the thicknesses of spin coated thin films are different on top of glass ($\sim$ 120 nm) and silver ($\sim$ 129 nm). This behaviour was systematic on all SU-8 based thin films used in the experiments.

The second silver layer with the same thickness of 38 nm was evaporated on top of the cured resist layer using same parameters as in the first evaporation. The whole structure is finished by spin coating a protective SU-8 thin film on top of the second silver layer using the spin speed 6000 rpm for 60 seconds, following 3 min bake at $\sim 95^\circ$ C on hot plate and exposure with UV-lamp for 1 min. Examples of prepared cavities with different thicknesses and thus different resonance wavelengths can be seen in Fig. 19.

Transmittance of the prepared cavities were measured with Perkin Elmer UV-vis spectrophotometer before making measurements with rotational set-up. Measured transmittance spectra of the cavities used in experiments can be seen in Fig. 20. The

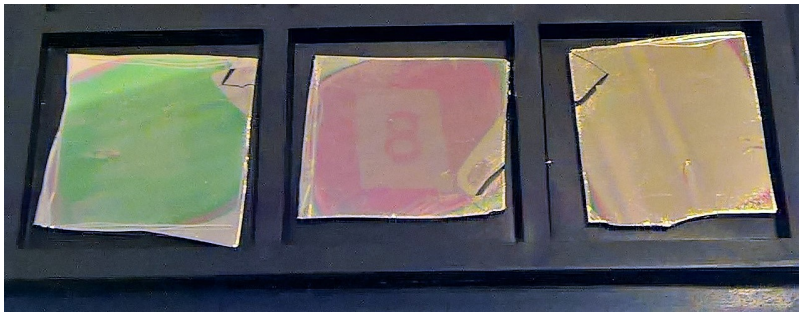

Figure 19. Examples of cavities prepared during process optimization. Cavities have different thicknesses and thus different resonance wavelengths.

plasma frequency of silver remains the same with different cavities having maximum transmittance at 330 nm. The 140 mM R6G cavity has slightly smaller transmittance at silver's plasma frequency hinting of slightly thicker silver layers. Q-factor is calculated for all cavities from the bare cavity. Q-factor is defined in equation (19) as a function of frequency. Same definition is valid for energy. Bare cavity's resonance energy is $E_r = 2.27$ eV. FWHM is obtained from Voigt peak fit giving FWHM = 0.164 eV. Therefore the quality factor of prepared cavities is approximately

$$Q = \frac{E_r}{\delta E} = \frac{2.27\,\text{eV}}{0.164\,\text{eV}} = 13.841... \approx 14. \tag{27}$$

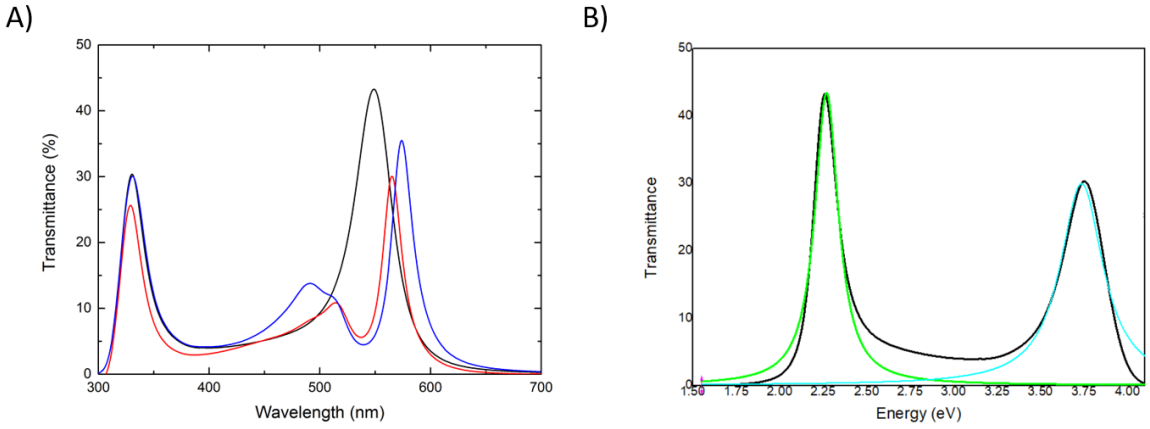

Figure 20. A) The transmittance spectra of optical cavities: (black curve) cavity without dye (called bare cavity), (red curve) 140 mM R6G cavity and (blue curve) 275 mM R6G cavity B) The transmittance spectrum of the bare cavity with 129 nm thick SU-8 layer and 38 nm thick silver layers has $E_r = 2.27$ eV and FWHM is = 0.164 eV according to Voigt peak fit (green curve). Voigt fit (cyan curve) to silver's plasma peak.

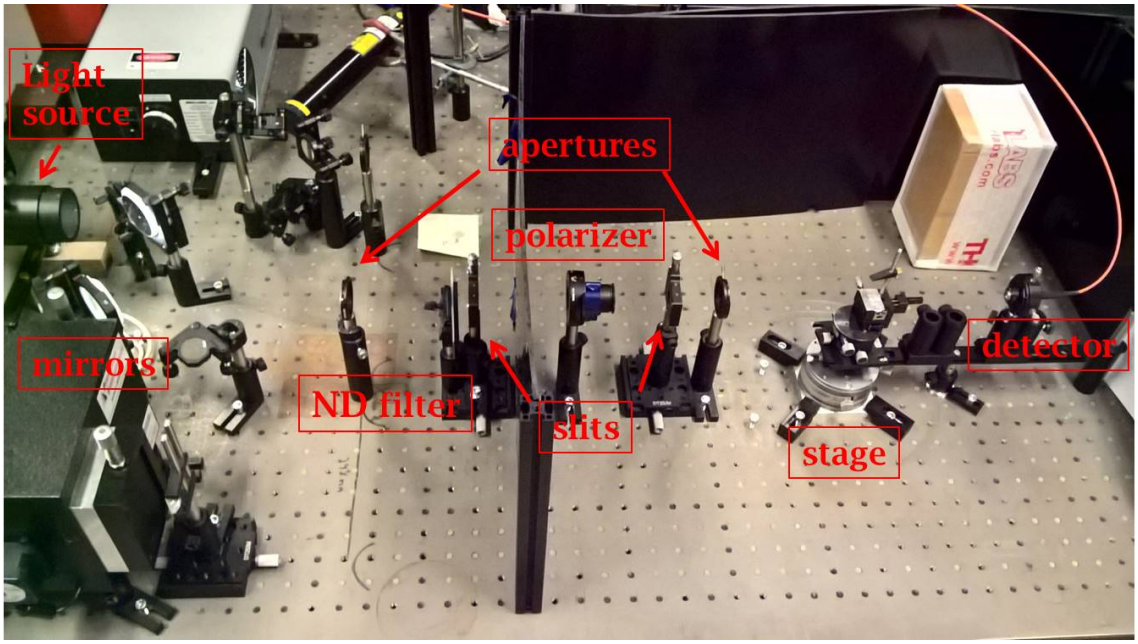

Figure 21. The set-up for optical spectroscopy with rotational stage.

3.4 Optical measurements

Perkin Elmer UV-vis spectrometer was used to confirm the transmittance resonances of the cavities at the normal incidence. Same spectrometer was also used to measure the absorbance of the thin films. Transmittance (T) can be converted into absorbance (Abs) using equation

$$Abs = -\log(T) \tag{28}$$

and vice versa absorbance can be converted into transmittance using equation

$$T = 10^{-Abs}. \tag{29}$$

While these conversions are useful it should be remembered, that absorbance is most often used in situations which have negligible reflectance. If sample has significant reflectance, absorption is better unit to use.

Image of the rotational optical measurement setup can be seen in Fig. 21. White light is produced by a halogen lamp. Using two mirrors and two slits light is collimated and aligned. ND filter is used to allow exposure time of 0.3 s while lamp is used with power of 150 W. Two apertures are used to decrease the spot size on the sample. Polarization of incident light is adjusted using a Glan Taylor reversible prism polarizer. The incident angle of light is controlled manually by rotating the goniometric mount, on which sample is attached. All optical components were purchased from Thorlabs. The signals are collected by a collimating optics assembly F220SMA-A (Thorlabs), which is connected by an optic fiber to Jobin Yvon iHR320 spectrometer equipped with Jobin Yvon Symphony CCD camera.

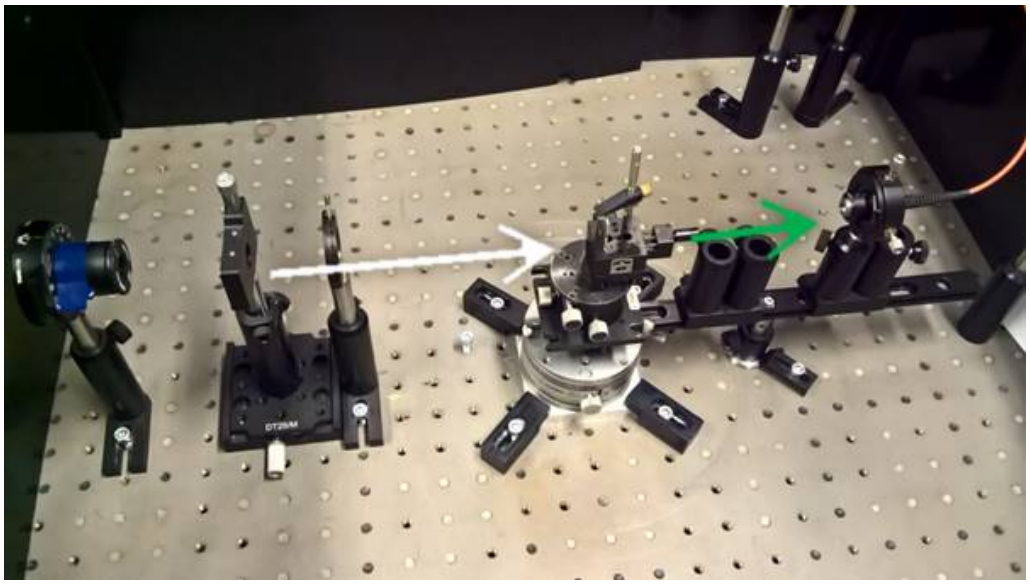

Figure 22. The setup for transmittance measurement. White light is incident to the cavity with tunable angle and only resonance wavelengths are transmitted directly. Detection is always in line with the incident light.

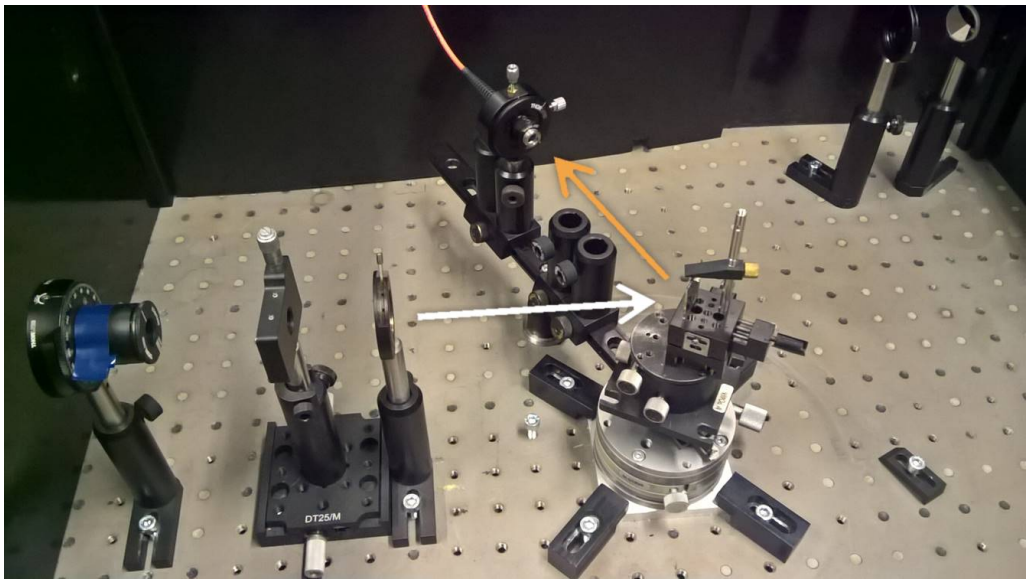

Figure 23. The same setup used for reflectance measurement. Cavities were placed on the holder so, that top mirror is facing the detector and glass substrate is towards the transmittance direction. In the image white light is incident to the cavity at 40° angle.

The rotational set-up with transmittance measurement is seen in Fig. 22. Same set-up is used to measure reflectance in Fig. 23. The angle of incident light is defined in respect to the normal of the cavity. Using this geometry 0° angle means, that light is incident perpendicular to the surface of the sample and transmittance is measured perpendicular to the surface of the sample. In used set-up reflectance can not be measured below 5 °angles.

In both transmittance and reflectance measurement Jobin Yvon spectrometer measures the intensity of transmitted I_t or reflected I_r light. Lamp intensity I_0 was measured for each measurement set. Transmittance and reflectance were calculated using equations

$$T = \frac{I_t}{I_0}, \quad R = \frac{I_r}{I_0}. \tag{30}$$

The transmittance of glass substrate T_a was measured at different angles. For each cavity (or thin-film) measurement T_m the transmittance of glass at corresponding angle is subtracted using equation

$$T_c = \frac{T_m}{T_a}, \tag{31}$$

in which T_c is the transmittance of only the cavity (or thin-film). In reabsorption measurements the glass substrates of all added thin-films are subtracted from the measured transmittance T_m using equation

$$T_r = \frac{T_m}{T_a \cdot (T_G)^n}, \tag{32}$$

in which T_G is the transmittance of glass at 0° angle, n is the amount of glasses on the path of light after the cavity and T_r is the transmittance of cavity combined with the added thin films. The reflectance spectra of cavities were always measured so, that the glass substrate was facing the transmittance direction and therefore was not on the path of measured light.

Both Perkin Elmer and Jobin Yvon spectrometers measure intensity against wavelength. Conversion from wavelength to energy is done using equation

$$E = \frac{hc}{\lambda}. \tag{33}$$

In calculations the easiest conversion is derived from (34) as

$$E(\text{eV}) = \frac{1240}{\lambda(\text{nm})}. \tag{34}$$

Since intensities are measured with respect to lamp spectra results are transmittance, reflectance or absorbance. Therefore there is no need for Jacobian transformation, which is needed in photoluminescence spectroscopy [53].

Only *s*-polarized light was used while measuring cavities, since the dispersion of cavities depends on the polarization of incident light. As was illustrated in Fig. 8 in section 2.2, a split can be obtained in spectra when measuring with unpolarized light. An example of transmittance measurement with unpolarized light with the bare cavity is seen in Fig. 24. The upper transmittance mode, resulting from *s*-polarized light, is 200 meV higher in energy at 70° than the transmittance mode of *p*-polarized light. Also, surface plasmon polaritons can not be excited to silver with *s*-polarized light.

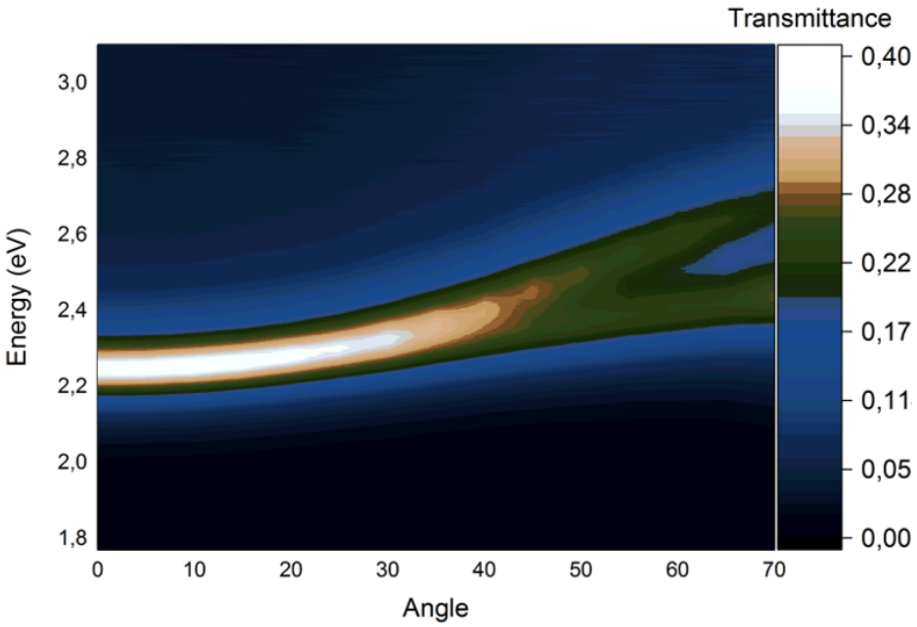

Figure 24. Transmittance dispersion of the bare cavity measured with unpolarized light. The upper mode is from incident *s*-polarized light and lower mode from *p*-polarized light.

4 Results

This section is divided in to three parts. First linear reabsorption is studied with bare cavity and R6G thin films. After understanding the origin of the split in the spectra in a noninteracting system, these results are compared to an interacting system, i.e. cavity with dyes. To understand the differences between the non-interacting reabsorbing system and the interacting cavity, a spectral comparison is made. Finally, the effect of increasing the concentration of the dye in the cavity is spectroscopically verified.

4.1 Linear reabsorption

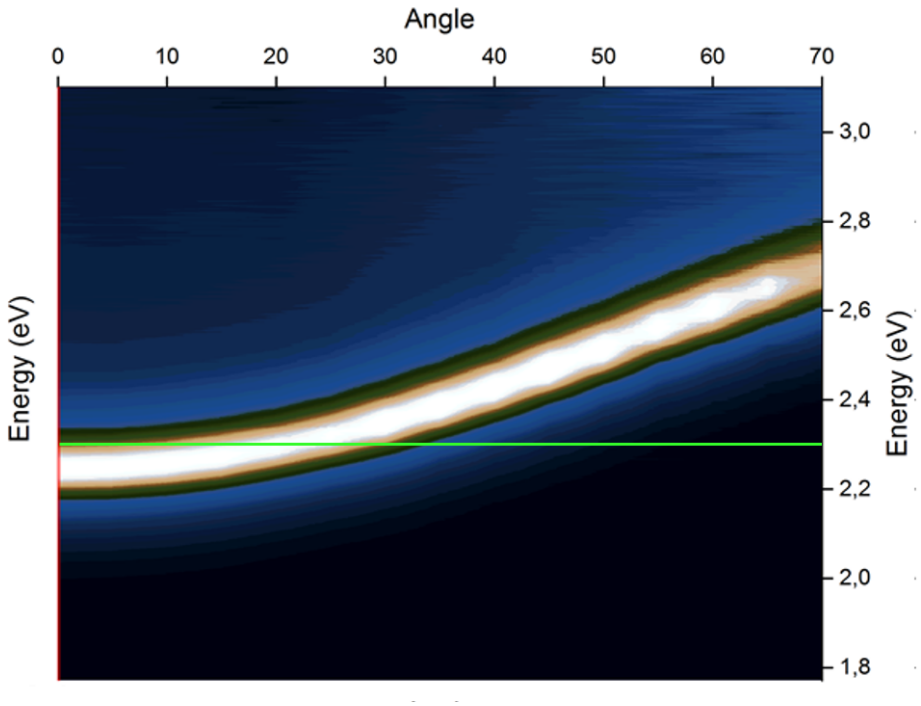

Figure 25. Transmittance dispersion of the bare cavity as a contour plot. The maximum absorbance of the stacked R6G films at 2.305 eV is drawn with a green line

Transmittance dispersion of the bare cavity is seen in Fig. 25. The green line indicates maximum absorbance of the stacked R6G films at 2.305 eV. The best overlap between the absorption line and cavity's transmittance dispersion is seen

at 20° angle geometry. Therefore all reabsorption measurements are performed at 20° angle. The quality factor of the bare cavity was calculated to be $Q = 14$ at 0° angle of incidence. Since the FWHM of the resonance remains approximately the same but the resonance energy increases with increasing angle, the quality factor of cavity increases. As is seen in Fig. 26, resonance energy is 2.27 eV at 0° angle with FWHM 0.164 eV. At 70° angle resonance energy has increased to 2.71 eV, but FWHM has increased only to 0.136 eV, giving quality factor

$$Q_{70} = \frac{2.71\,\text{eV}}{0.136\,\text{eV}} = 19.926... \approx 20. \tag{35}$$

The increase of quality factor is insignificant in this study.

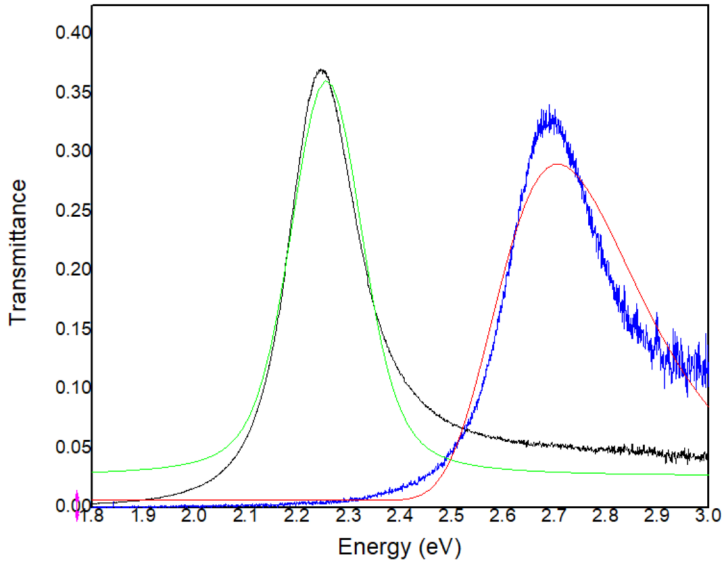

Figure 26. (Black curve) resonance mode of bare cavity at 0° angle and (green curve) Voigt fit to the mode. (Blue curve) resonance mode at 70° incident angle and (red curve) Asym2Sig fit to the mode.

In Fig. 27 A) we see the system in which R6G films are inserted in the path of light, which is transmitted through a bare cavity. The maximum transmittance of the bare cavity is 36.2 % at 2.29 eV without R6G films in the transmittance path. The absorbance of the R6G thin films increase (see Fig. 14) as more films are stacked. Thus total transmittance of the system consisting of the cavity and the stacked films decreases. Most of the light is absorbed at the maximum transmittance of the bare cavity, since it matches the absorption maximum of R6G. For easier comparison the absorbance of the R6G films in Fig. 14 is converted to transmittance using equation (36)

$$T = 10^{-Abs}. \tag{36}$$

The transmittance spectra of stacked R6G films are shown in Fig. 27 B).

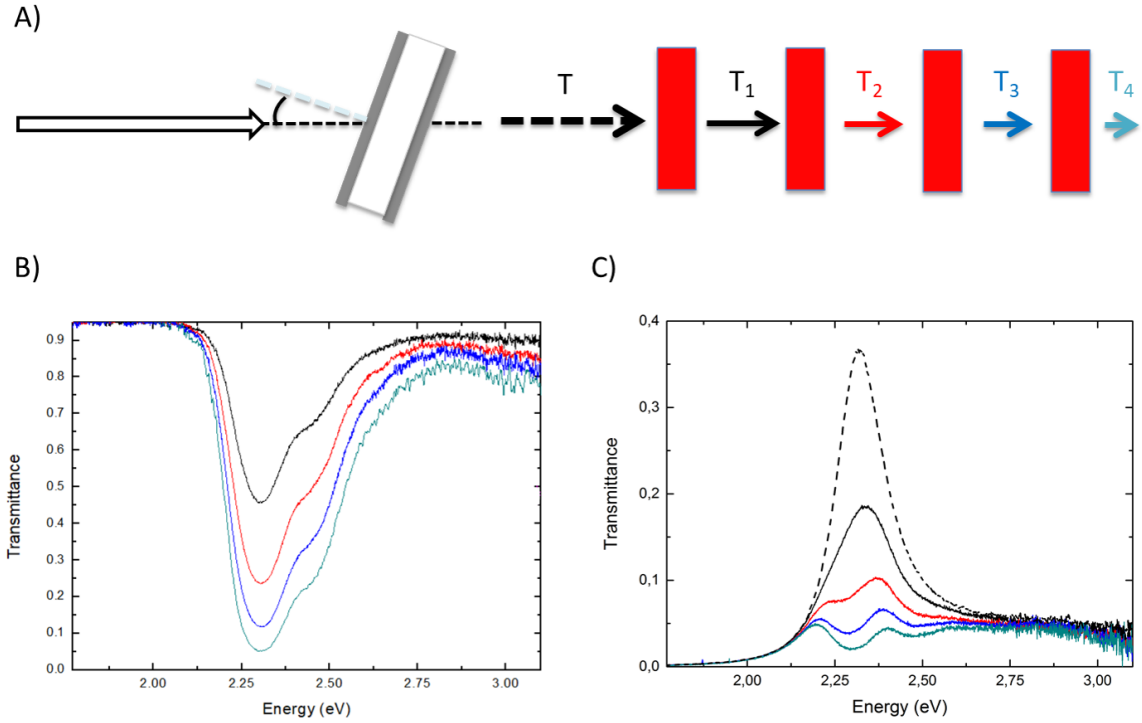

Figure 27. A) cavity was set at 20° orientation. R6G films were added after the cavity to absorb the transmitted light before reaching the detector. B) the transmittance spectra of the stacked R6G films, (black curve) one R6G thin film, (red curve) two R6G films, (blue curve) three R6G films and (cyan curve) four R6G thin films are stacked C) (dotted black curve) transmittance of bare cavity. Other colors represent the transmitted light through cavity and the same amount of R6G thin films as in B).

As can be seen in Fig. 27 C), only the total transmittance seems to drop when the first R6G film is inserted on the path of light after the bare cavity. After a second R6G film is inserted a split starts to develop in spectrum. A clear split is observed after the third R6G film is inserted and the split gets even greater after the fourth thin film. Thus a split in the transmittance spectrum can be achieved by linear reabsorption and falsely a Rabi split of 200 meV could be interpreted from the spectrum. It is clear from the experimental set-up, that the system is completely non-interacting. Therefore we can at ease deduce, that transmittance is not a suitable parameter to measure Rabi split in spectroscopy.

Because measuring only transmittance is not suitable method to validate strong coupling, a reflectance measurement is also carried out. Measurement method is presented in Fig. 28 A). The transmittance of the stacked R6G films is seen in Fig.

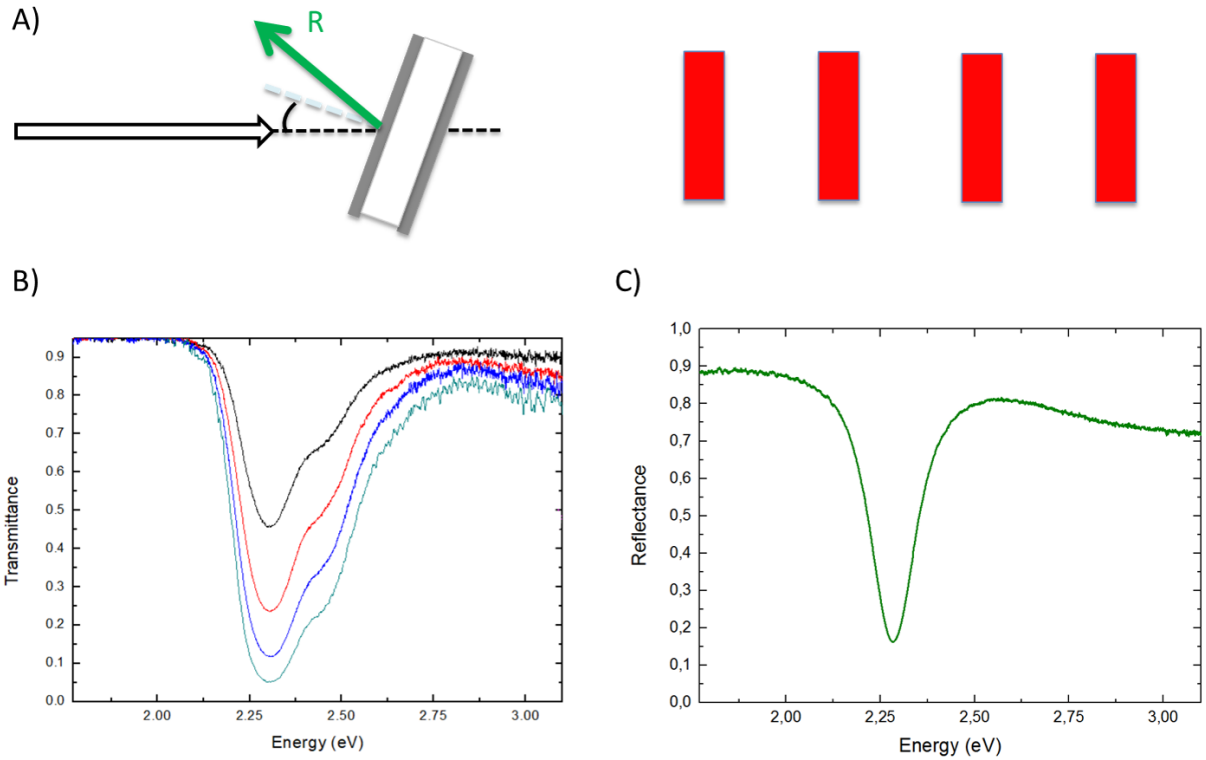

Figure 28. A) cavity was set at 20° orientation. R6G films have no effect on the reflectance of the bare cavity B) the transmittance spectra of stacked R6G films, (black curve) one R6G thin film, (red curve) two R6G films, (blue curve) three R6G films and (cyan curve) four R6G thin films are stacked C) (green curve) reflectance of the bare cavity

28 B) and the reflectance spectrum of the bare cavity is seen in Fig. 28 C). It is clear that the reflectance spectrum of the bare cavity remains the same no matter how many R6G films are inserted at the transmittance path. Spectrum has the resonance mode with minimum reflectance 16.2 % at 2.28 eV.

Knowing both transmittance and reflectance, the absorption spectra of the reabsorbing cavity system can be calculated using equation 21

$$A = 1 - T - R$$

As an example the absorption of bare cavity is plotted with transmittance and reflectance in Fig. 29. The transmittance of the bare cavity is 36.4 % at 2.28 eV and reflectance is 16.2 % meaning, that absorption of the bare cavity is 47.4 % at 2.28 eV. Part of light is absorbed by the silver layers and substantially smaller part is absorbed by the SU-8 layer. Part of light is also scattered by surface roughnesses.

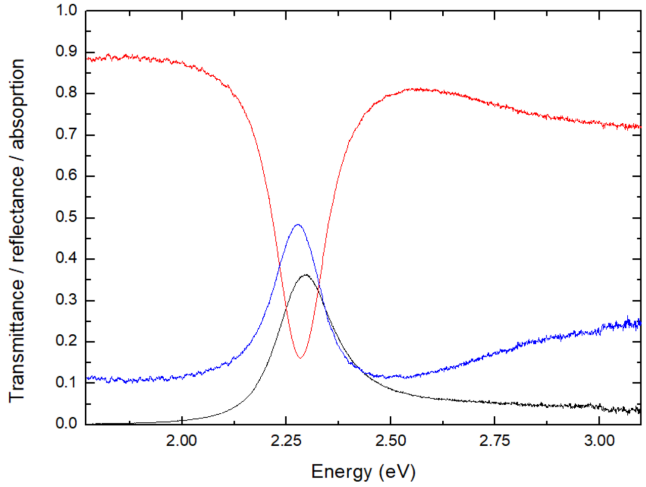

Figure 29. (Blue curve) Absorption spectrum of the bare cavity at 20° geometry. (Black curve) transmittance and (red curve) reflectance are also shown. Absorption is shifted to lower energy because of the small mismatch between transmittance and reflectance maxima.

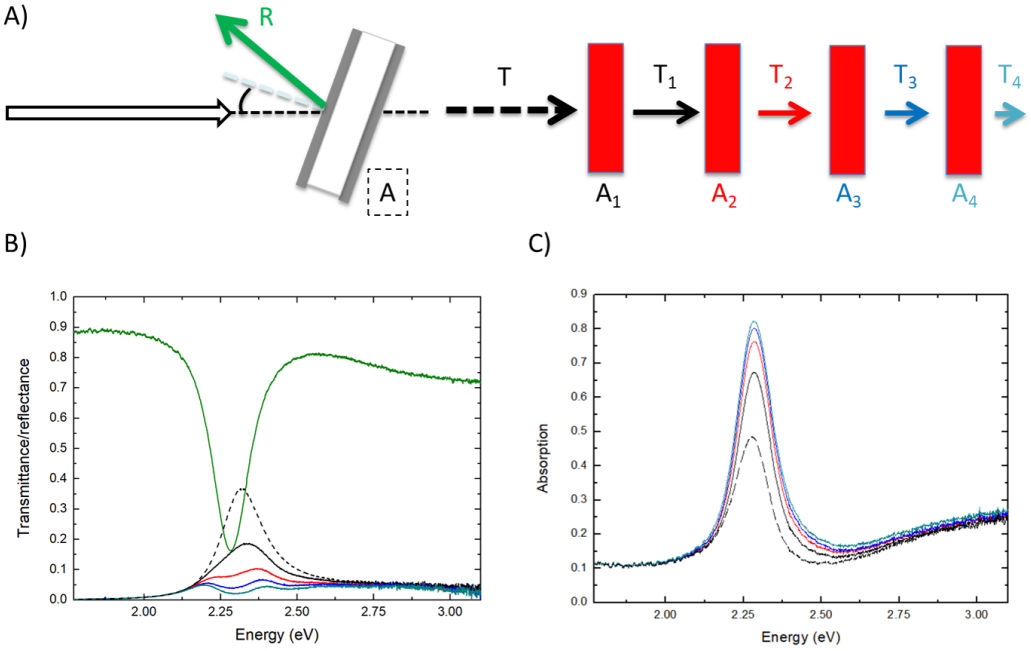

Figure 30. A) All spectral components when cavity is set to 20° orientation B) the transmittance the bare cavity with (black curve) one R6G thin film, (red curve) two R6G films, (blue curve) three R6G films and (cyan curve) four stacked R6G thin films and (green curve) the reflectance spectrum of bare cavity C) (dotted black curve)absorption of bare cavity. Other colors show the absorption of the system with same amount of R6G thin films as in B).

All of the spectral components of the reabsorbing system are seen in Fig. 30 A). The reabsorption results of transmittance and reflectance measurements with the stacked R6G thin-films are combined in Fig.30 B). The absorption of reabsorbing system is calculated for different amounts of R6G thin films using equation (21) and the spectra are seen in Fig. 30 C). Even though the transmittance spectrum of reabsorbing system show a clear split with three and four stacked R6G films, there is no split seen in the absorption! For easier comparison the transmittance spectra of the R6G films are converted to absorption assuming that reflectance of the thin film is negligible and therefore using equation

$$A = 1 - T.$$

This way the effect of increasing absorption in R6G films can be directly compared to the absorption of the whole reabsorbing system. The comparison is seen in Fig.31. The absorption of reabsorbing system increases in similar manner to the increase of the absorption of the stacked R6G films. A clear observation from reabsorption measurements is, that combined absorption of bare cavity and stacked R6 films doesn't have a split, no matter how many R6G films are stacked behind the bare cavity. The total absorption merely increases due to the increasing absorption of the stacked R6G films. The absorption of the bare cavity is 47.4 % at 2.28 eV. The total absorption of the cavity and R6G films is shifted to 2.285 eV because of the mismatch of 275 mM R6G film's maximum absorbance at 2.305 eV and the bare cavity's transmittance and reflectance maximum and minimum, respectively, at 2.28 eV. Absorption is increased to 67.4 %, then 76.5 %, following 80.2 % and finally to 82.2 % with four R6G films. Conclusion is, that observing a split in the transmittance or reflectance spectra is not evidence of strong coupling.

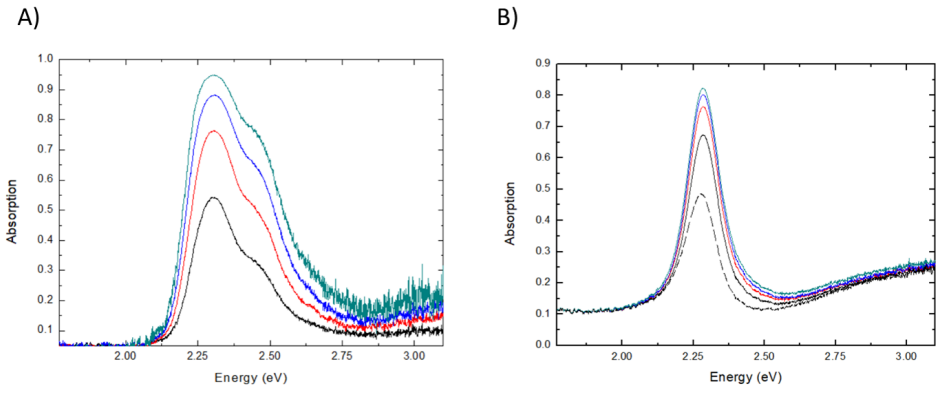

Figure 31. A) the absorption spectra of (black curve) one R6G thin film, (red curve) two R6G films, (blue curve) three R6G films and (cyan curve) four stacked R6G thin films B) (dotted black curve)absorption of bare cavity. Other colors show the absorption of the system with same amount of R6G thin films as in A).

4.2 Strongly coupled system

A non-interacting system was investigated in the previous section. In the 140 mM R6G cavity SU-8 layer is doped with dye molecules, which interact with cavity photons. This coupled system is measured to conform strong coupling and to make a spectral comparison to the noninteracting system. The transmittance dispersion of the 140 mM R6G cavity is seen in Fig. 32. The dispersion of the interacting cavity is seen to follow that of bare cavity (white dots), but there is a clear split in the spectrum. The maximum absorbance of 140 mM R6G thin film is plotted as a green vertical line at 2.31 eV. The 20° geometry has again the best resonance according to the transmittance dispersion. The maximum fluorescence of 140 mM R6G film is presented as a red line.

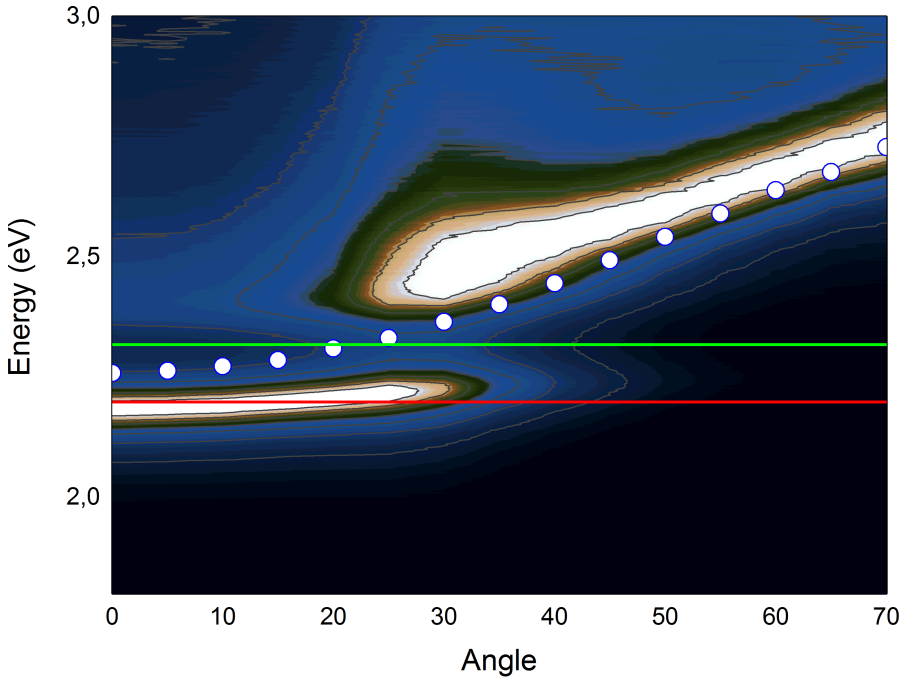

Figure 32. Transmittance dispersion of the 140 mM R6G cavity as a contour plot. (White dots) transmittance dispersion of the bare cavity, (green line) maximum absorbance of the R6G 140 mM film and (red line) maximum fluorescence of the same film.

The transmittance spectrum of the bare cavity with four R6G films on the transmittance path and the transmittance spectrum of the 140 mM R6G cavity at 20° geometry are compared in Fig. 33. Both systems clearly have a split with minimum transmittance at 2.305 eV, which is R6G film's absorbance maximum. Obvious difference between the spectra is seen in the amount of transmittances. The 140 mM cavity's transmittance decreases compared to the bare cavity's maximum transmittance of 36 %; the higher polariton has maximum transmittance 18 % at 2.42 eV

and the lower polariton has transmittance 25 % at 2.21 eV. Yet, the transmittance of the bare cavity on the fake lower polariton is only 5 % at 2.20 eV and on the fake higher polariton 5 % at 2.40 eV. The transmittance of the reabsorbing system drops significantly due to high amount of absorption from the R6G films.

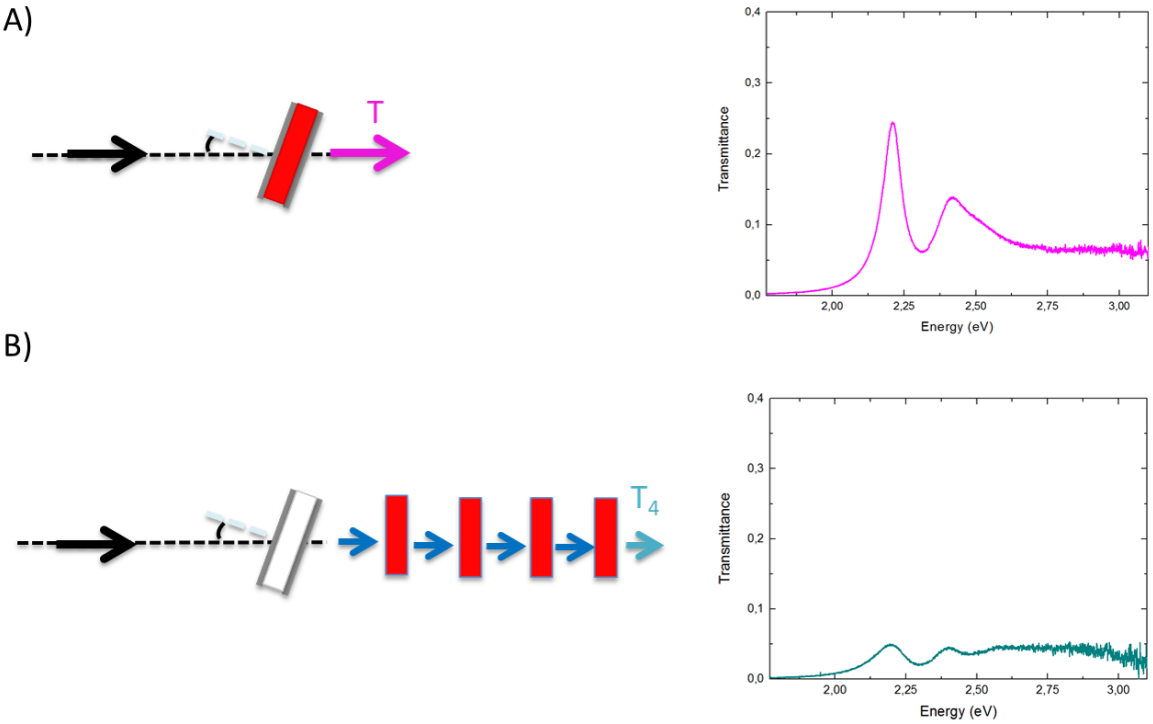

Figure 33. A) 140 mM R6G cavity's transmittance spectrum in 20° angle shows a clear split B) the transmittance spectrum of the system consisting of the bare cavity and four R6G films on the path of light has also split but the transmittance peaks are much weaker.

Reflectance spectra of systems are compared in Fig. 34. As was pointed in the previous section, the bare cavity does not have a split in the reflectance spectrum. The bare cavity's reflectance has resonance, and thus the minimum, 16 % at 2.28 eV. 140 mM R6G cavity has minimum reflectance 40 % for lower polariton at 2.22 eV and 52 % at 2.39 eV for higher polariton. The "Rabi split" could be interpreted to be 110 meV, which is less than the value given by transmittance measurement.

From the combined spectra in Fig. 35 the differences between the reabsorbing system and the 140 mM R6G cavity can be investigated easily. Both systems show a split in their transmittance spectra, but only interacting system gives a split in the reflectance measurement and especially in the absorption calculation. The 140

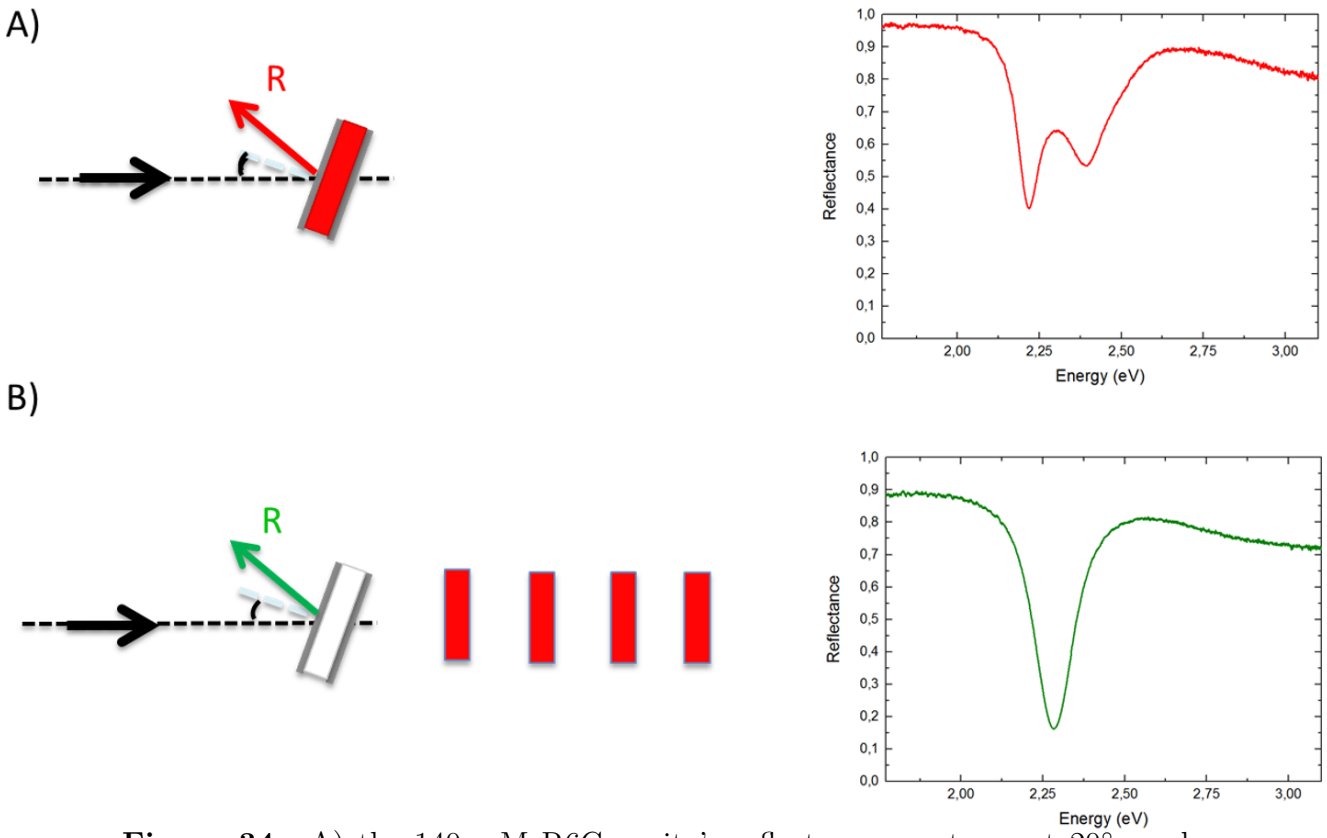

Figure 34. A) the 140 mM R6G cavity's reflectance spectrum at 20° angle shows a clear split B) only the resonance mode is seen in the reflectance of the bare cavity.

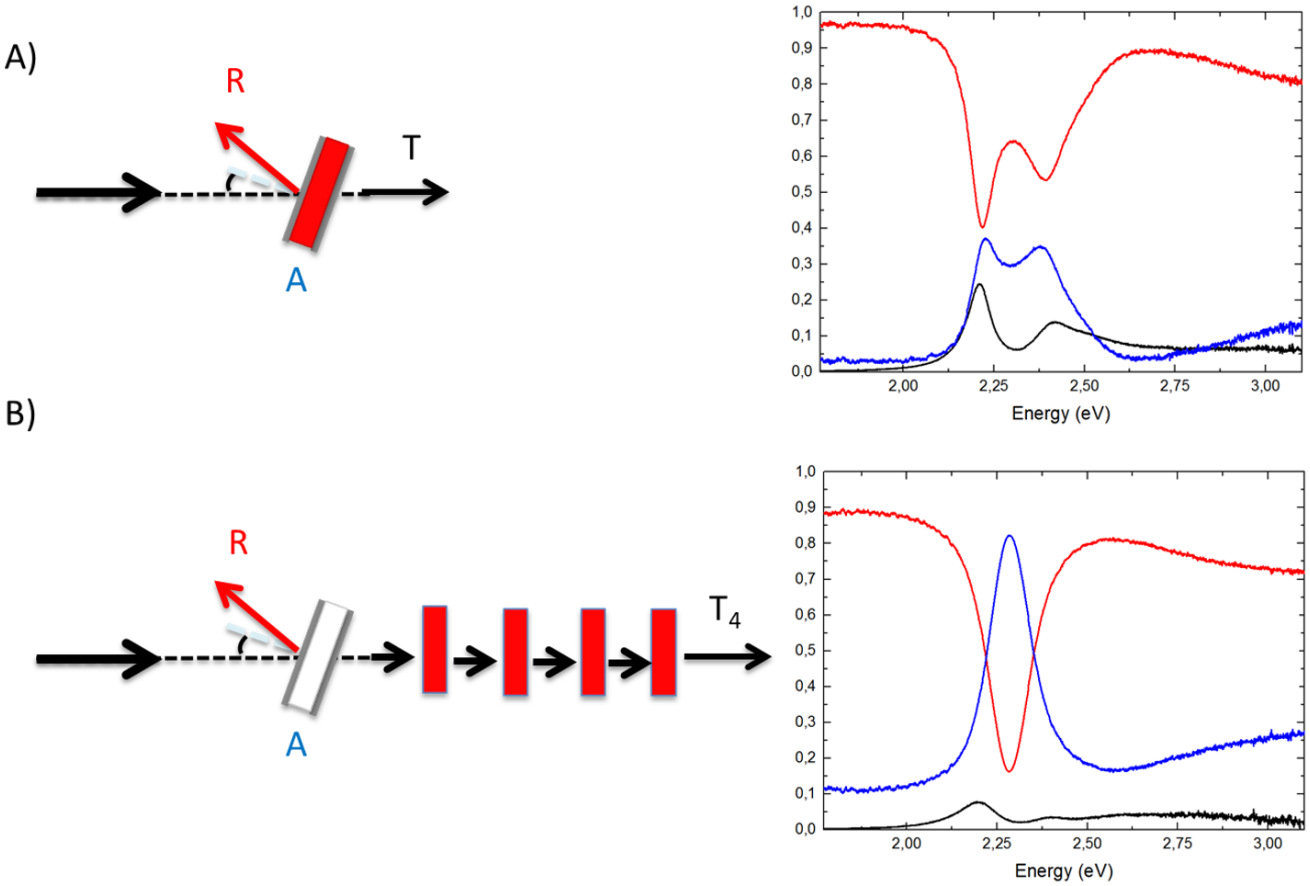

Figure 35. A) the 140 mM R6G cavity at 20° angle and its (black curve) transmittance, (red curve) reflectance, (blue curve) absorption spectrum . B) reabsorbing system at 20° angle and its, (black curve) transmittance, (red curve) reflectance, (blue curve) absorption spectrum.

mM cavity has absorption maximum 37 % at 2.23 eV for lower polariton and 35 % at 2.38 eV for higher polariton. Real Rabi split of the 140 mM cavity is thus 150 meV. The absorption spectra is the ultimate fingerprint for strong coupling in spectroscopy, as has been pointed out in literature [35, 20].

Even if the R6G films in the reabsorption system were relocated to the reflectance measurement the amount of absorbed light would be exactly same as in transmittance measurement. Therefore the split would cancel in absorption calculation. This phenonemon was also observed by Houdré in 1993 [50] and the idea was presented in Fig. 13. Even stronger confirmation for the system being strongly coupled can be achieved by observing the concentration dependence of the system.

4.3 Concentration dependence

In the previous section it was spectroscopically proven that the material excitons of R6G and the cavity photons indeed form a strongly coupled system resulting in polaritons. To observe the change of the vacuum Rabi split a cavity with higher concentration of R6G was prepared and characterized. As was pointed out in equation (26), the vacuum Rabi split should increase with increasing concentration of molecules in the cavity. The dispersion of the 275 mM R6G cavity can be seen in Fig. 36. Dispersion follows that of the bare cavity, which is marked with white dots, as was the case with the 140 mM cavity. Higher polariton widens dramatically at higher angles, which is an indication of the second Rabi splitting starting to form. With even higher concentrations a second split would be observed in spectra at the shoulder of the R6G's absorbance. The split between the polariton branches is clearly bigger at 20° than in the 140 mM cavity. The maximum absorbance of the 275 mM R6G thin film is plotted as a green vertical line and maximum fluorescence of the same film is presented as a red line.

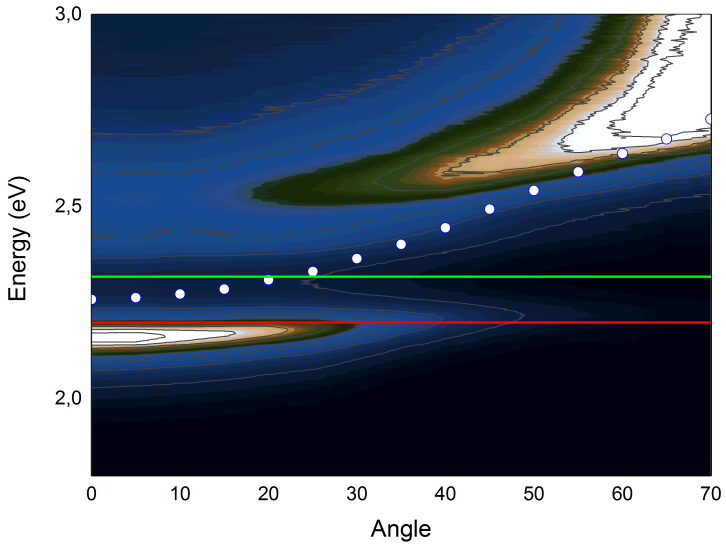

Figure 36. Transmittance dispersion of the 275 mM R6G cavity as a contour plot. (White dots) transmittance dispersion of the bare cavity, (green line) maximum absorbance of the 275 mM R6G thin-film and (red line) maximum fluorescence of the same film.

Increasing the concentration of the molecules inside the cavity should increase the vacuum Rabi-split, as is shown in equation (26). The absorption of the bare cavity, the 140 mM R6G cavity and the 275 mM R6G cavity are compared in Fig. 37. The backgrounds of the systems are not aligned due to the differences in the systems (meaning thickness of the film, possible variation in mirror thickness in either side

of the thin-film, heterogenous of the thin films) and the measurement error of the set-up used. Yet, the increase of the split in the spectra is easy to observe.

For the 275 mM R6G cavity maximum absorption of the lower polariton is 50 % at 2.18 eV. The maximum absorption of the higher polariton is 54 % at 2.40 eV. Rabi split of the 275 mM R6G cavity is thus 220 meV. From the bare cavity's no split at all vacuum Rabi split increases to 150 meV in the 140 mM R6G cavity and to 220 meV in the 275 mM R6G cavity. Unfortunately, a third concentration of strongly coupled cavity couldn't be prepared making validation of equation (26) impossible with only two measured points.

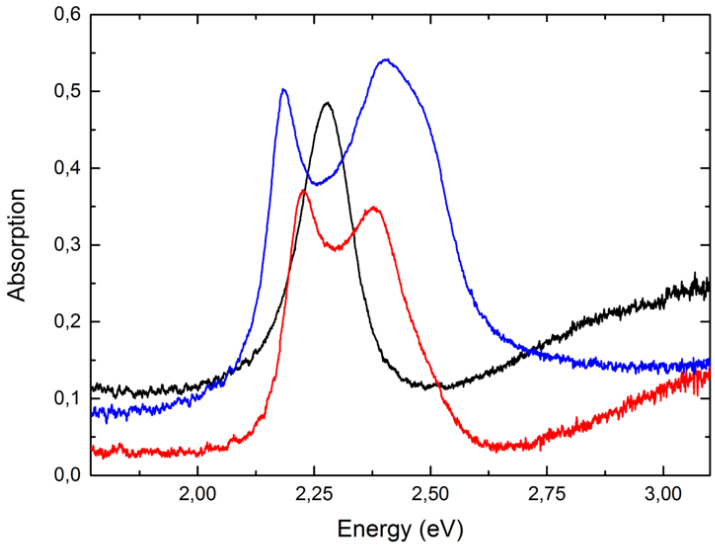

Figure 37. Absorbance of the cavities: (Black curve) bare cavity, (red curve) 140 mM R6G cavity and (blue curve) 275 mM R6G cavity.

5 Conclusions

The aim of this thesis is to illustrate the spectroscopic differences between a strongly coupled and a non-interacting system, which has a split in the spectrum. The researched systems in this thesis are microcavities with R6G dye molecules. To illustrate the properties of cavities and to find a suitable cavity system, simulations were made using the transfer matrix method. Both increasing the thickness of the medium or the real part of the refractive index of the medium in a cavity lower the resonance energy of the cavity. Increasing the thickness of silver mirror layers lowers the amount of transmitted light but also increases the quality factor of the cavity. *S*-polarized light is better in cavity measurements, since the dispersion is greater than with *p*-polarized light and there is no possibility to excite surface plasmon polaritons (SPP) on the silver mirrors. A split was obtained in the spectra with purely classical model. On the other hand, the refractive index holds inside it all the quantum information of the optical properties of the material and papers have been published with purely classical modeling of strong coupling [34, 54]. As is discussed for SPP strong coupling [4] and cavity strong coupling [35], the strong coupling regime between light and matter can be described with classical, semiclassical or pure quantum description and all treatments yield same concentration dependence within a low excitation regime.

Bare cavity and R6G doped cavities were prepared to compare linear reabsorption and strongly coupled cases. According to the simulations the cavities were prepared with 38 nm silver layers and 129 nm thick medium with a protective resist layer on top of the upper mirror. Prepared cavities had low quality factor of approximately 14. A split in the bare cavity's dispersion spectrum was induced by measuring dispersion with unpolarized light. A non-interacting system can show a split with a reabsorption arrangement in transmittance measurement.

Cavities weren't perfectly synced with the absorption of R6G. R6G has absorbance maximum at 535 nm while the transmittance maximum of bare the cavity was at 549 nm. To obtain the greatest split in the reabsorption tests the measurements had to be made with the bare cavity in 20° angle. The reflectance was measured with the same angle. Also R6G doped cavities showed maximum Rabi split with 20 ° angle of the incident light.

As was shown in experiments, only R6G doped cavities had a split in the absorption spectra. These peaks are a result from the lower and upper polariton in the system. As has been shown in earlier experiments, measuring absorption of the system is the correct way to distinguish strongly coupled systems. Therefore it was confirmed,

that strong coupling was achieved at room temperature in a low quality microcavity. By increasing the concentration of R6G in a cavity from 140 mM to 275 mM, vacuum Rabi splitting measured from the absorption spectra increased from 150 meV to 220 meV. The linear dependence of square root of concentration to vacuum Rabi split could not be researched, since at least third concentration would have been needed.

Radically increasing the thickness of one of the mirrors makes an asymmetrical system, which does not transmit light at all. Simulation of the system and required experiments simplify, because only reflectance and absorption have to be considered. Another improvement would be preparing so called sandwich structures in cavities. These structures would guarantee, that excitons are not interacting with the mirror material.

The strong coupling strength should be measured from the wave-vector dispersion, not the angle dispersion, as is pointed out in the experiments by Symonds *et. al* [55]. The minimum energy splitting in angle does not correspond to the energy splitting at the resonance wave-vector. Using the angle as the parameter to determine the Rabi splitting results in an overestimation of the strength of the coupling.

References

[1] E. M. Purcell. Spontaneous Emission Probabliities at Radio Frquencies. *Physical Review*, 69:674–674, 1946.

[2] Serge Haroche and Daniel Kleppner. Cavity quantum electrodynamics. *Physics Today*, 42(1):24–30, 1989.

[3] Th Förster. Zwischenmolekulare Energiewanderung und Fluoreszenz. 33:166–175, 1948.

[4] P. Törmä and W. L. Barnes. Strong coupling between surface plasmon polaritons and emitters: a review. *Reports on progress in physics. Physical Society (Great Britain)*, 78(1):013901, 2015.

[5] Simon Gröblacher, Klemens Hammerer, Michael R Vanner, and Markus Aspelmeyer. Observation of strong coupling between a micromechanical resonator and an optical cavity field. *Nature*, 460(7256):724–727, 2009.

[6] J. P. Long and B. S. Simpkins. Coherent coupling between a molecular vibration and fabry-perot optical cavity to give hybridized states in the strong coupling limit. *ACS Photonics*, 2(1):130–136, 2015.

[7] Jino George, Atef Shalabney, James A. Hutchison, Cyriaque Genet, and Thomas W. Ebbesen. Liquid-phase vibrational strong coupling. *Journal of Physical Chemistry Letters*, 6(6):1027–1031, 2015.

[8] Christof P. Dietrich, Anja Steude, Laura Tropf, Marcel Schubert, Nils M. Kronenberg, K. Ostermann, Sven Höfling, and Malte C. Gather. An exciton-polariton laser based on biologically produced fluorescent protein. *arXiv*, (August):1601.06983, 2016.

[9] Rohit Chikkaraddy, Bart De Nijs, Felix Benz, Steven J Barrow, Oren A Scherman, and Peter Fox. Single-molecule strong coupling at room temperature in plasmonic nanocavities. *Nature*, 535:127–130, 2016.

[10] James A. Hutchison, Tal Schwartz, Cyriaque Genet, Eloïse Devaux, and Thomas W. Ebbesen. Modifying chemical landscapes by coupling to vacuum fields. *Angewandte Chemie - International Edition*, 51(7):1592–1596, 2012.

[11] James A. Hutchison, Andrea Liscio, Tal Schwartz, Antoine Canaguier-Durand, Cyriaque Genet, Vincenzo Palermo, Paolo Samor, and Thomas W. Ebbesen. Tuning the work-function via strong coupling. *Advanced Materials*, 25(17):2481–2485, 2013.

[12] Y. Kaluzny, P. Goy, M. Gross, J. M. Raimond, and S. Haroche. Observation of self-induced Rabi oscillations in two-level atoms excited inside a resonant cavity: The ringing regime of superradiance. *Physical Review Letters*, 51(13):1175–1178, 1983.

[13] C. Weisbuch, M. Nishioka, A. Ishikawa, and Y. Arakawa. Observation of the coupled exciton-photon mode splitting in a semiconductor quantum microcavity. *Physical Review Letters*, 69(23):3314–3317, 1992.

[14] A. Pawlis, A. Khartchenko, O. Husberg, D. J. As, K. Lischka, and D. Schikora. Large room temperature Rabi-splitting in II-VI semiconductor microcavity quantum structures. *Microelectronics Journal*, 34(5-8):439–442, 2003.

[15] Gabriel Christmann, Raphaël Butté, Eric Feltin, Anas Mouti, Pierre A. Stadelmann, Antonino Castiglia, Jean François Carlin, and Nicolas Grandjean. Large vacuum Rabi splitting in a multiple quantum well GaN-based microcavity in the strong-coupling regime. *Physical Review B - Condensed Matter and Materials Physics*, 77(8):1–9, 2008.

[16] D. Lidzey, D. Bradley, T. Virgili, a. Armitage, M. Skolnick, and S. Walker. Room Temperature Polariton Emission from Strongly Coupled Organic Semiconductor Microcavities. *Physical Review Letters*, 82(16):3316–3319, 1999.

[17] D. G. Lidzey, D. D. C. Bradley, M. S. Skolnick, T. Virgili, S. Walker, and D. M. Whittaker. Strong exciton-photon coupling in an organic semiconductor microcavity. *Nature*, 395(6697):53–55, 1998.

[18] D. G. Lidzey, T. Virgili, D. D.C. Bradley, M. S. Skolnick, S. Walker, and D. M. Whittaker. Observation of strong exciton-photon coupling in semiconductor microcavities containing organic dyes and J-aggregates. *Optical Materials*, 12(2):243–247, 1999.

[19] Javier Galego, Francisco J. Garcia-Vidal, and Johannes Feist. Many-molecule reaction triggered by a single photon in polaritonic chemistry. *Physical Review Letters*, 119(September):1–6, 2017.

[20] Tal Schwartz, James A. Hutchison, Cyriaque Genet, Stefan Haacke, and Thomas W. Ebbesen. Polariton dynamics under strong light-molecule coupling. *ChemPhysChem*, 14(1):125–131, 2013.

[21] Antoine Canaguier-Durand, Eloïse Devaux, Jino George, Yantao Pang, James A. Hutchison, Tal Schwartz, Cyriaque Genet, Nadine Wilhelms, Jean Marie Lehn, and Thomas W. Ebbesen. Thermodynamics of molecules strongly coupled to the vacuum field. *Angewandte Chemie - International Edition*, 52(40):10533–10536, 2013.

[22] Shaojun Wang, Thibault Chervy, Jino George, James A. Hutchison, Cyriaque Genet, and Thomas W. Ebbesen. Quantum Yield of Polariton Emission

from Hybrid Light-Matter States. *The Journal of Physical Chemistry Letters*, 5(8):1433–1439, 2014.

[23] Thomas W. Ebbesen. Hybrid Light-Matter States in a Molecular and Material Science Perspective. *Accounts of Chemical Research*, 49(11):2403–2412, 2016.

[24] Gulis Zengin, Tina A. Gschneidtner, Ruggero Verre, Lei Shao, Tomasz J. Antosiewicz, Kasper Moth-Poulsen, Mikael Käll, and Timur Shegai. Evaluating Conditions for Strong Coupling Between Nanoparticle Plasmons and Organic Dyes Using Scattering and Absorption Spectroscopy. *The Journal of Physical Chemistry C*, 2016.

[25] Gülis Zengin, Martin Wersäll, Sara Nilsson, Tomasz J. Antosiewicz, Mikael Käll, and Timur Shegai. Realizing strong light-matter interactions between single-nanoparticle plasmons and molecular excitons at ambient conditions. *Physical Review Letters*, 114(15):1–14, 2015.

[26] Svitlana Baieva, Ossi Hakamaa, Gerrit Groenhof, Tero T Heikkila, and J Jussi Toppari. Dynamics of Strongly Coupled Modes between Surface Plasmon Polaritons and Photoactive Molecules: The Effect of the Stokes Shift. 2017.

[27] Mikko A. Koponen, Ulrich Hohenester, Tommi K. Hakala, and J. Jussi Toppari. Absence of mutual polariton scattering for strongly coupled surface plasmon polaritons and dye molecules with a large Stokes shift. *Physical Review B - Condensed Matter and Materials Physics*, 88(8):1–8, 2013.

[28] J. Dintinger, S. Klein, F. Bustos, W. L. Barnes, and T. W. Ebbesen. Strong coupling between surface plasmon-polaritons and organic molecules in subwavelength hole arrays. *Physical Review B - Condensed Matter and Materials Physics*, 71(3):1–5, 2005.

[29] E. Orgiu, J. George, J. A. Hutchison, E. Devaux, J. F. Dayen, B. Doudin, F. Stellacci, C. Genet, J. Schachenmayer, C. Genes, G. Pupillo, P. Samorì, and T. W. Ebbesen. Conductivity in Organic Semiconductors Hybridized with the Vacuum Field. *Nature Materials*, 14:1123–1129, 2015.

[30] David M Coles, Niccolo Somaschi, Paolo Michetti, Caspar Clark, Pavlos G Lagoudakis, Pavlos G Savvidis, and David G Lidzey. Polariton-mediated energy transfer between organic dyes in a strongly coupled optical microcavity. *Nature materials*, 13(7):712–9, 2014.

[31] Xiaolan Zhong, Thibault Chervy, Shaojun Wang, Jino George, Anoop Thomas, James A. Hutchison, Eloise Devaux, Cyriaque Genet, and Thomas W. Ebbesen. Non-Radiative Energy Transfer Mediated by Hybrid Light-Matter States. *Angewandte Chemie - International Edition*, 55(21):1–6, 2016.

[32] Kerry J Vahala. Optical microcavities. *Nature*, 424(6950):839–846, 2003.

[33] David M Coles, Yanshen Yang, Yaya Wang, Richard T Grant, Robert A Taylor, Semion K Saikin, Alán Aspuru-Guzik, David G Lidzey, Joseph Kuo, Hsiang

Tang, and Jason M Smith. Strong coupling between chlorosomes of photosynthetic bacteria and a confined optical cavity mode. *Nature Communications*, 5:5561, 2014.

[34] Yifu Zhu, Daniel J. Gauthier, S. E. Morin, Qilin Wu, H. J. Carmichael, and T. W. Mossberg. Vacuum Rabi splitting as a feature of linear-dispersion theory: Analysis and experimental observations. *Physical Review Letters*, 64(21):2499–2502, 1990.

[35] R. Houdré. Early stages of continuous wave experiments on cavity-polaritons. *Physica Status Solidi (B) Basic Research*, 242(11):2167–2196, 2005.

[36] Jino George, Shaojun Wang, Thibault Chervy, Antoine Canaguier-Durand, Gael Schaeffer, Jean-Marie Lehn, James a. Hutchison, Cyriaque Genet, and Thomas W. Ebbesen. Ultra-strong coupling of molecular materials: spectroscopy and dynamics. *Faraday Discuss.*, 178:281–294, 2015.

[37] Anton Kuzyk, Mika Pettersson, J Jussi Toppari, Tommi K Hakala, Hanna Tikkanen, Henrik Kunttu, and Päivi Törmä. Molecular coupling of light with plasmonic waveguides. *Optics Express*, 15(16):9908–9917, 2007.

[38] T. K. Hakala, J. J. Toppari, A. Kuzyk, M. Pettersson, H. Tikkanen, H. Kunttu, and P. Törmä. Vacuum rabi splitting and strong-coupling dynamics for surface-plasmon polaritons and rhodamine 6G molecules. *Physical Review Letters*, 103(5):1–4, 2009.

[39] Jianmin Shi, Xianping Zhang, and Douglas C. Neckers. Xanthenes: fluorone derivatives. 1. *The Journal of Organic Chemistry*, 57:4418–4421, 1992.

[40] B Harbecke. Coherent and Incoherent Reflection and Transmission of Multilayer Structures. *Applied Physics B*, 39:165–170, 1986.

[41] M S Skolnick, T a Fisher, and D M Whittaker. Strong coupling phenomena in quantum microcavity structures. *Semiconductor Science and Technology*, 13(7):645–669, 1999.

[42] Steven J. Byrnes. Multilayer optical calculations. *arXiv:1603.02720*, page 21, 2016.

[43] P. B. Johnson, R. W. Christy, and Optical Constants. Optical Constants of the Noble Metals. *Physical Review B*, 6(12):4370–4379, 1972.

[44] V.B. Braginsky, M.L. Gorodetsky, and V.S. Ilchenko. Quality-factor and nonlinear properties of optical whispering-gallery modes. *Physics Letters A*, 137(7):393–397, 1989.

[45] W Leupacher and a Penzkofer. Refractive-index measurement of absorbing condensed media. *Applied optics*, 23(10):1554, 1984.

[46] H J Kimble. Strong interactions of single atoms and photons in cavity QED Strong Interactions of Single Atoms and Photons in Cavity QED. *Physica Scripta*, T76:127–137, 1998.

[47] Salvatore Gambino, Marco Mazzeo, Armando Genco, Omar Di Stefano, Salvatore Savasta, Salvatore Patane, Dario Ballarini, Federica Mangione, Giovanni Lerario, Daniele Sanvitto, and Giuseppe Gigli. Exploring Light-Matter Interaction Phenomena under Ultrastrong Coupling Regime. *ACS Photonics*, 1(10):1042–1048, 2014.

[48] I Pockrand, A Brillante, and D Möbius. Exciton-surface plasmon coupling : An experimental investigation. *Journal of Chemical Physics*, 77(12):6289–6295, 1982.

[49] V. Savona, L. C. Andreani, P. Schwendimann, and A. Quattropani. Quantum well excitons in semiconductor microcavities: Unified treatment of weak and strong coupling regimes. *Solid State Communications*, 93(9):733–739, 1995.

[50] R. Houdré, R. P. Stanley, U. Oesterele, M. Ilegems, and C. Weisbuch. Room temperature exciton-photon Rabi splitting in a semiconductor microcavity. *Le Journal de Physique IV*, 03(C5):51–58, 1993.

[51] Microchem. SU-8 2000 Permanent Epoxy Negative Photoresist. Technical report, 2015.

[52] L. V. Levshin, M. G. Reva, and B. D. Ryzhikov. Effect Of Intermolecular Interactions On The Electronic Spectra Of R6G. *translation from Zhurnal Prikladnoi Spektroskopii*, 26(1):66–70, 1977.

[53] Patanjali Kambhamptai. Get the Basics Right: Jacobian Conversion of Wavelength and Energy Scales for Quantitative Analysis of Emission Spectra. *Journal of Physical Chemistry Letters*, 4(2):3316–3318, 2013.

[54] Lukas Novotny. Strong coupling, energy splitting, and level crossings: A classical perspective. *American Journal of Physics*, 78(11):1199, 2010.

[55] C. Symonds, C. Bonnand, J. C. Plenet, A. Bréhier, R. Parashkov, J. S. Lauret, E. Deleporte, and J. Bellessa. Particularities of surface plasmon-exciton strong coupling with large Rabi splitting. *New Journal of Physics*, 10, 2008.

A Thin film solution calculation

Used SU-8 (SU-8 2100 MicroChem, Lot# 05080635) has 75 percent solids and density $\rho_{SU8} = 1.237$ g/ ml [51]. The density of SU-8 2100 with solid percent 100 % is calculated to be $\rho_{SU8-DRY} = 1.304$ g/ ml given the solid% versus density increase in data sheet. Since SU-8 is diluted to one sixth with cyclopentanone (meaning there is 1 part SU-8 for 6 parts of cyclopentanone), the SU-8 root solutions have solid content S_{SU8} of

$$S_{SU8} = \frac{\rho_{SU8} \cdot 0.75}{7} = \frac{1.237\,\mathrm{g/ml} \cdot 0.75}{7} = 0.132536\,\mathrm{g/ml}. \tag{37}$$

The SU-8 root solution was prepared by mixing 1.984 g SU-8 2100 solution with 9.623 ml cyclopentanone. The volume of added SU-8 is

$$V_{SU8} = \frac{1.984\,\mathrm{g}}{1.237\,\mathrm{g/ml}} = 1.60388\,\mathrm{ml}. \tag{38}$$

The solid content of root solution can be confirmed to be

$$S_{SU8} = \frac{1.984\,\mathrm{g} \cdot 0.75}{1.60388\,\mathrm{ml} + 9.623\,\mathrm{ml}} = 0.132539\,\mathrm{g/ml}. \tag{39}$$

140 mM R6G thin film is prepared by mixing 150 µl 14 mM R6G in ethanol solution with 170 µl cyclopentanone and 150 µl SU-8 root solution, which had been diluted 1:6 by volume with cyclopentanone. The solid content of the 140 mM film's solution is calculated as following: 150 µl 14 mM R6G in ethanol-solution contains the solid mass m_{R6G1} of R6G

$$m_{R6G1} = C_{R6G} \cdot M_{R6G} \cdot V_{R6G} = 0.014\,\mathrm{mol/l} \cdot 479.02\,\mathrm{g/mol} \cdot 0.15\,\mathrm{ml} = 1.0059\,\mathrm{mg} \tag{40}$$

and solid mass of SU-8 in the final solution is

$$m_{SU8} = S_{SU8} \cdot V_{SU8} = 0.132539\,\mathrm{g/ml} \cdot 150\,\mathrm{\mu l} = 19.875\,\mathrm{mg}. \tag{41}$$

Therefore the solid content, which effects the thin film's thickness, of the solution before spin coating is

$$S_{140mM} = \frac{m_{SU8} + m_{R6G}}{V_{SU8} + V_{R6G} + V_{cyclop.}} = \frac{1.0059\,\mathrm{mg} + 19.875\,\mathrm{mg}}{150\,\mathrm{\mu l} + 150\,\mathrm{\mu l} + 170\,\mathrm{\mu l}} = 44.43\,\mathrm{mg/ml}. \tag{42}$$

The concentration of the ready thin film is approximated

$$C_{140mM} = \frac{m_{R6G}/M_{R6G}}{m_{SU8}/\rho_{SU8-DRY}} = \frac{1.0059\,\mathrm{mg}/479.02\,\mathrm{g/mol}}{19.875\,\mathrm{mg}/1.304\,\mathrm{g/ml}} = 0.137781\,\mathrm{mol/l}. \tag{43}$$

To make a R6G doped thin film with arbitrary concentration I choose concentration of the film $C_{275mM} = 275$ mM, amount of R6G to be used $m_{R6G} = 2$ mg and the concentration of dye solution $C_{R6G} = 28$ mM. To obtain approximately same thickness to the films, solid content of the film has to be $S_{275mM} = 44.43$ mg/ml. First I calculate the mass of SU-8 from the concentration of the film

$$m_{SU-8} = \frac{\rho_{SU8-DRY} \cdot m_{R6G}}{C_{275mM} \cdot M_{R6G}} = \frac{1.304\,\mathrm{g/ml} \cdot 2\,\mathrm{mg}}{0.26\,\mathrm{mol/l} \cdot 479.02\,\mathrm{g/mol}} = 0.019798\,\mathrm{g} \tag{44}$$

volume of SU-8 solution is easy to calculate knowing the mass

$$V_{SU8} = \frac{m_{SU8}}{S_{SU8}} = \frac{0.019798\,\mathrm{g}}{0.132539\,\mathrm{g/ml}} = 0.149419\,\mathrm{ml}. \tag{45}$$

The volume of dye solution is fixed by choosing the mass of R6G and the concentration of the dye solution

$$V_{R6G} = \frac{m_{R6G}}{C_{R6G} \cdot M_{R6G}} = \frac{2\,\mathrm{mg}}{0.028\,\mathrm{mol/l} \cdot 479.02\,\mathrm{g/mol}} = 0.149114\,\mathrm{ml}. \tag{46}$$

The volume of cyclopentanone is used to obtain the required solution for the given film

$$V_{cyclop.} = \frac{m_{SU8}}{S_{275mM}} - V_{SU8} + \frac{m_{R6G}}{S_{275mM}} - V_{R6G}$$

$$V_{cyclop.} = \frac{19.798\,\mathrm{mg}}{44.4275\,\mathrm{mg/ml}} - 0.149419\,\mathrm{ml} + \frac{2\,\mathrm{mg}}{44.4275\,\mathrm{mg/ml}} - 0.149114\,\mathrm{ml}$$

$$V_{cyclop.} = 0.192109\,\mathrm{ml}.$$

so the volumes used for preparing a 275 mM R6G thin film are 150 µl SU-8, which has been diluted 1:6 by volume with cyclopentanone, 150 µl 28 mM R6G solution and 192 µl cyclopentanone.